JCI The Journal of Clinical Investigation

Cytomegalovirus mediates expansion of IL-15-responsive innate-memory cells with SIV killing function

Gema Méndez-Lagares, … , Peter A. Barry, Dennis J. Hartigan-O'Connor

J Clin Invest. 2021. https://doi.org/10.1172/JCI148542.

Research In-Press Preview **Immunology** **Infectious disease**

Graphical abstract

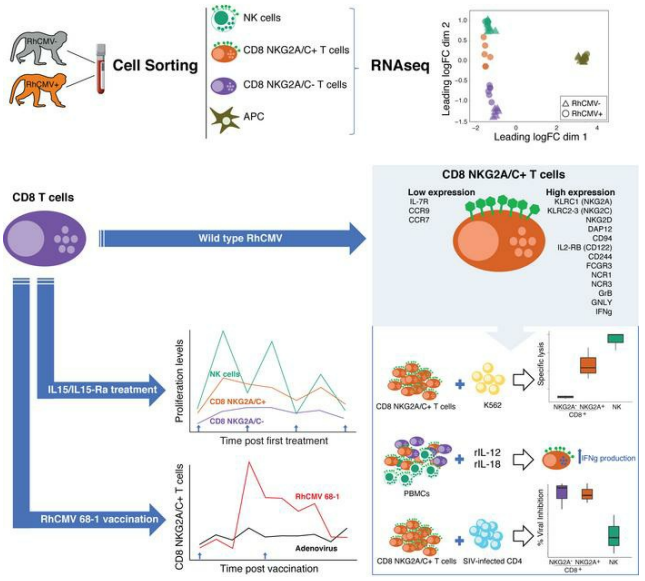

Find the latest version:

https://jci.me/148542/pdf

TITLE

Cytomegalovirus mediates expansion of IL-15-responsive innate-memory cells with SIV killing function

Authors:

Gema Méndez-Lagares[1,2], Ning Chin[1,2], W.L. William Chang[1,2], Jaewon Lee[3,4], Míriam Rosás-Umbert[5], Hung T. Kieu[1,2], David Merriam[1,2], Wenze Lu[1,2], Sungjin Kim[2,4], Lourdes Adamson[4], Christian Brander[5,6,7], Paul A. Luciw[1,4,8], Peter A. Barry[1,4,8,] and Dennis J. Hartigan-O'Connor[1,2,9]

Affiliations:

[1]California National Primate Research Center, University of California, Davis, CA 95616, USA

[2]Department in Medical Microbiology and Immunology, University of California, Davis, CA 95616, USA

[3]Graduate Group in Immunology, University of California Davis, Davis, CA 95616, USA

[4]Center for Immunology and Infectious Diseases, University of California Davis, Davis, CA 95616, USA

[5]IrsiCaixa - AIDS Research Institute, Badalona, Barcelona, Spain.

[6]Universitat de Vic-Universitat Central de Catalunya (UVic-UCC), Vic, Barcelona, Spain.

[7]Institució Catalana de Recerca i Estudis Avançats (ICREA), Barcelona, Spain.

[8]Department of Pathology and Laboratory Medicine, University of California, Davis, CA 95616, USA

[9]Division of Experimental Medicine, Department of Medicine, University of California, San Francisco, CA 94110, USA

Running title: Innate-memory T cell expansion by CMV

Corresponding author: Dennis J. Hartigan-O'Connor, Department of Medical Microbiology and Immunology, UC Davis, School of Medicine, One Shields Avenue, Davis, CA 95616-8816, Phone (530) 752-9402, **Email address:** dhartigan@ucdavis.edu

Keywords: rhesus macaques, CMV, NKG2A, transcriptome, vaccines

ABSTRACT

Inter-individual immune variability is driven predominantly by environmental factors including exposure to chronic infectious agents such as cytomegalovirus (CMV). We investigated the effects of rhesus CMV (RhCMV) on composition and function of the immune system in young macaques. Within months of infection, RhCMV was associated with impressive changes in antigen presenting cells, T cells, and NK cells—and marked expansion of innate-memory $CD8^+$ T cells. These cells express high levels of NKG2A/C and the IL-2- and IL-15-receptor beta chain, CD122. IL-15 was sufficient to drive differentiation of the cells *in vitro* and *in vivo*. Expanded NKG2A/$C^+CD122^+CD8^+$ T cells in RhCMV-infected macaques, but not their NKG2-negative counterparts, were endowed with cytotoxicity against class I-deficient K562 targets and prompt IFN-ɣ production in response to stimulation with IL-12 and IL-18. Because RhCMV clone 68-1 forms the viral backbone of RhCMV-vectored SIV vaccines, we also investigated immune changes following administration of RhCMV 68-1-vectored SIV vaccines. These vaccines led to impressive expansion of NKG2A/C^+CD8^+ T cells with capacity to inhibit SIV replication *ex vivo*. Thus, CMV infection and CMV-vectored vaccination drive expansion of functional innate-like CD8 cells *via* host IL-15 production, suggesting that innate-memory expansion could be achieved by other vaccine platforms expressing IL-15.

INTRODUCTION

The human and nonhuman primate immune responses vary markedly within outbred populations, both phenotypically and functionally. Of significant medical importance, people mount variable immune responses to vaccines and infectious challenges (1, 2). It is perhaps surprising that immune variation in humans is primarily driven by environmental factors (3). For example, we and others have shown that gut microbiota composition has a significant and long-lasting impact on immune development (4-6). Chronic viral infections such as those caused by cytomegalovirus (CMV) (3) form another class of environmental exposure that alters the host immune system. Interestingly, the activity of sub-clinical infection with some viruses varies with host immunosuppression, resulting in a complex relationship between these infections and other factors affecting host immunity (7).

CMV is a β-herpesvirus that infects a large proportion of the adult human population, having an average global seroprevalence of 83% (8). The virus has a large genome (~236 kbp) with multiple immunomodulatory gene functions affecting host intrinsic, innate, and adaptive functions (>33% of the genomic coding capacity; ref. (9). Collectively, these viral gene products enable the virus to establish and maintain a lifelong persistence within immune-competent hosts (10). Human CMV (HCMV) infection influences nearly 60% of all immune phenotypes and functional responses, including a major impact on the memory T-cell pool, with about 10% of the memory T-cell repertoire (both $CD4^+$ and $CD8^+$) being CMV-specific (11). This massive overall impact is perhaps most easily understood as the cumulative effect of lifelong expression of CMV-encoded immunomodulatory gene functions; therefore, the immunologic impact of CMV is considered by many to be categorically distinct from that of other viruses. However,

another non-exclusive possibility is that the host response to CMV exaggerates mechanisms that are also at play in other viral infections.

HCMV infection is associated with expansion of and adaptive changes in subsets of NK cells, e.g., “g-negative NK cells” or “g^-NK” cells, a class of cells with memory function that do not rely on germline-encoded, antigen-specific receptors (12). Some investigators have argued that these cells are essentially specific to CMV infection, since CMV-seronegative individuals with prevalent g-NK cells can frequently be shown to possess CMV-specific T cells. HCMV infection is also associated with expansion of adaptive immune cells with innate features, e.g., NK-CTLs, which are $CD8^+$ cytotoxic T lymphocytes (CTLs) with ‘NK-like’ surface markers and functional activity. NK-CTLs express HLA class I-specific inhibitory receptors most often associated with NK cells (e.g., NKG2A) and have the capacity to kill many allogeneic tumor cells, apparently due to recognition of HLA-E-restricted allogeneic peptides (13-16). HCMV-infected cells markedly downregulate the surface expression of HLA class Ia molecules (ligands for HLA class I-specific inhibitory NK receptors) (17). HLA-E-restricted NK-CTL may thus provide an additional source of effector cells capable of lysing such class Ia-deficient targets (17).

Other $CD8^+$ T cells with an NK-like surface phenotype (KIR, NKG2A) have been identified in human PBMCs (18-20). Jacomet et al. (20) argued that those cells may represent the equivalent of murine “innate/memory” $CD8^+$ T cells also known as virtual memory CD8 T (T_{VM}) cells (reviewed in ref. (21). In a recent study, Jin et al. (22) demonstrated a critical role for T_{VM} cells in controlling the HIV reservoir through KIR- but not TCR-mediated recognition. Importantly, generation of T_{VM} cells is dependent on IL-15 signaling. T_{VM} express IL-15Rβ (CD122 or IL2Rβ) (23) and eomesodermin (Eomes), a T-box

transcription factor that promotes IL-15Rβ expression (24). T_{VM} cells also exhibit increased responsiveness to IL-12 and IL-18, which together promote cytokine production and even bystander killing from T_{VM} in an antigen-independent manner (25, 26). While T_{VM} cells lack access to the gut, they preferentially migrate to the liver to gain access to IL-15 (26). Recently, a third subset of innate-like human $CD8^+$ T cells was identified, which expresses an array of NK-associated proteins and has antimicrobial activity against intracellular pathogens (amCTLs; ref (27). amCTLs additionally express granzyme B (GZMB), perforin (PRF), and granulysin (GNLY), as well as IL2Rβ. Interestingly, the authors found that epidermal Langerhans cells (LCs) can induce naïve $CD8^+$ T cells to differentiate into am-CTLs (27).

CMV-vectored HIV vaccines were developed to exploit the unique and inimitable features of CMV-encoded immunomodulation. Salient characteristics of CMV include (1) the ability to reinfect hosts with prior CMV immunity, (2) viral-mediated persistence in hosts with vigorous anti-CMV immune responses, and (3) a large and manipulatable viral genome capable of expressing ectopic antigen cassettes (28). In the rhesus macaque model, rhesus cytomegalovirus- (RhCMV-) vectored SIV (RhCMV/SIV) vaccines were shown to provide unprecedented protection against SIV disease in ~50% of recipient macaques (29-33). Remarkably, protection is associated in many cases with complete clearance of the pathogenic challenge virus, a feat that in humans has only rarely been achieved after bone-marrow transplant (34). RhCMV/SIV vaccines are based on a specific strain of RhCMV, 68-1, carrying several mutations compared to the wild-type virus that confer altered cell tropism (9). RhCMV-vectored vaccines provoke robust adaptive immune response to vaccine antigens driven by both MHC Class II and especially HLA-E-restricted CD8 T-cell responses (35, 36). Notably, RhCMV-vectored vaccines retain much

of the immunomodulatory character associated with wild-type RhCMV infection, and thus, act broadly on the host immune system.

At present, it remains unclear if such a broad impact on the host immune system could be an important part of the mechanism of protection mediated by RhCMV-vectored vaccines. To investigate how RhCMV infection impacts upon the rhesus immune system, we explored RhCMV-mediated immune modulation at the protein and transcript level in immune cells of RhCMV-seropositive versus -seronegative macaques. Dramatic expansion of NKG2A/C^{+}CD8^{+} T cells was observed in animals infected by both wild-type and 68-1 vaccine strains of RhCMV. The transcriptomic profile of the expanded cells was more similar to that of NK cells than of NKG2A/C^{-} CTLs, including high expression of NK-associated surface markers, granzymes, granulysin, inflammatory cytokines, and cytokine receptors. In fact, the transcriptional profile extensively overlapped that described for T_{VM} cells (21) or amCTLs (27). Furthermore, NKG2A/C^{+} CD8^{+} T cells exhibited functional capacities that appeared identical to those of T_{VM} cells. Thus, wild-type and vaccine-strain RhCMV cause innate memory CD8^{+} T-cell expansion that may contribute to RhCMV/SIV-mediated protection against SIV.

RESULTS

Extensive effects of RhCMV infection on the macaque immune system

To investigate changes in cells of the circulating immune system associated with RhCMV infection, we characterized peripheral blood immunophenotypes in 42 RhCMV-seronegative (RhCMV-) and 29 RhCMV-seropositive (RhCMV+) juvenile rhesus macaques ranging in age from 5-10 months (Supplemental Table 1). The study animals were housed in outdoor corrals within their natal groups encompassing a broad range of ages (neonate to >20 years) in which RhCMV is endemic. Viral spread is mediated by horizontal transfer of virus in the bodily fluids of RhCMV-seropositive animals (saliva, urine) across mucosal surfaces of co-housed cohorts. Rhesus macaques rapidly seroconvert during the first year of life due to high levels of RhCMV shedding in bodily fluids of RhCMV-infected animals (37, 38). For the age range of animals in this study (5 – 10 months), prior reported seroprevalence data indicated that the frequency of seroprevalence would have been ~25% (5 months) - ~90% (10 months) (37). Accordingly, the RhCMV+ macaques in this study would have been infected relatively recently (weeks to months) prior to sample collection. Since both seronegative and seropositive animals were housed together in outdoor corrals, all animals would have been comparably exposed to most other endemic infectious agents.

We assessed blood for a comprehensive set of immunophenotypes defined by five cytometry panels including T, T_{reg}, NK, and antigen-presenting-cell (APC) markers and also tested the capacity for intracellular cytokine expression (gating strategies shown in Supplemental Figures 1-5). To summarize the variability in the dataset, we first performed principal component analysis (PCA). RhCMV+ and RhCMV- animals were shown to differ

substantially in several key components of the immune system, as demonstrated by almost complete separation of the two animal groups in a plot of the first two principal components (Figure 1A, *p* Adonis <0.001). Some rhesus macaques in our study were also infected with additional endemic viral pathogens, including simian foamy virus (SFV), rhesus rhadinovirus (RRV), and/or Macacine alphaherpesvirus 1 (i.e., simian herpes B virus - HERB). However, clear clusters were not observed when plotting according to infections with these viruses (Figure 1B).

Significant reduction of naïve T cells and accumulation of memory and, especially, effector cells were observed among RhCMV+ animals in both the $CD4^+$ and $CD8^+$ subsets (Figure 1C). This impact on immune homeostasis was accompanied by increased T cell proliferation ($Ki\text{-}67^+$) and activation ($CD38^+HLADR^+$), as well as increased capacity for cytokine production by T cells stimulated with PMA and Ionomycin (Figure 2, red or blue oval markers). As we have shown previously (1), only RhCMV+ animals developed circulating T cells capable of IL-4 expression, while simultaneously demonstrating higher frequencies of Th1 and Th17 T cells. Cellular activation and proliferation might be expected in all immune subsets as a natural inflammatory response to infection. Nonetheless, and although APCs (monocytes, myeloid and plasmacytoid dendritic cells) were more frequently represented among the PBMCs of RhCMV+ animals (Figure 2), expression of co-stimulatory molecules, especially CD83 and CD86, were substantially lower on these cells (Figure 2, purple oval markers, and Figure 1D) in the infected rhesus macaques. RhCMV+ animals also had more circulating NK cells (Figure 1E) and a significant increase in the abundance of $CD16^+$ compared to $CD56^+$ NK cells (Figure 1E). Finally, we observed an expansion of $CD3^+CD8^+$ T cells expressing NKG2A/C (Figure 1F), a cell population that has been reported to be expanded in certain HCMV-

seropositive individuals (14, 17). Note that the inhibitory NKG2A and activating NKG2C receptors of non-human primates are not distinguished by commercially available antibodies due to similarity of their extracellular domains (39). Approximately 60% of the $CD3^+CD8^+NKG2A/C^+$ expressed TCRαβ (average 60 ± 6.1). Thus, recent RhCMV infection (<~5 months) was associated with profound changes to a broad spectrum of the host immune systems of rhesus macaques.

Transcriptomes of APC $CD11c^+$ dendritic cells, NK cells, and $CD8^+$ T cells in RhCMV-seropositive vs. -seronegative animals

To better understand the immunologic changes imposed by RhCMV infection, we performed transcriptomic analysis by RNA 3' tag sequencing of fresh, flow-sorted, $CD11c^+$ dendritic cells ($CD3^-CD20^-$ HLA-DR^+CD11c^+), $NKG2A/C^-CD8^+$ T cells ($CD3^+CD20^-CD8^+NKG2A/C^-$), or NK cells ($CD3^-CD20^-CD8^+NKG2A/C^+$) from six RhCMV+ and six RhCMV- rhesus macaques (Table 1; Supplemental Figure 6A-C for sort strategy and purity checks). The average post-sort purity was 96.8% ± 1.9 for APC $CD11c^+$ dendritic cells, 99.1% ± 2.1 for $NKG2A/C^-CD8^+$ T cells, and 99.9% ± 0.1 for NK cells. Differential expression analyses were conducted using the limma-voom Bioconductor pipeline, using a statistical model incorporating the flow-sorted cell population, RhCMV serostatus, and fragmentation time. Standard errors of estimates were adjusted for within-animal correlation. Differentially expressed genes for a given contrast were defined to have an adjusted p-value of < 0.05.

The markers used for sorting were differentially expressed (DE) in the expected populations, confirming successful sorting. Other subset-specific markers were seen in the expected patterns, e.g., *Lck* and *ZAP70* in T cells but not dendritic cells. Subsequently

focusing on comparable cell subsets from RhCMV+ vs. RhCMV- animals, our analysis identified 411, 585, and 1371 protein-coding transcripts DE by sorted dendritic cells, NKG2A/C^{-}CD8^{+} T cells and NK cells, respectively, between RhCMV-infected and -uninfected animals (p_{adj}<0.05; Figure 3A). 64 genes were DE in all subsets, and in 63 cases, these differences were of the same direction. This shared gene expression prolife in different cell types demonstrated shared effects of RhCMV across cellular subsets. KEGG enrichment analyses were performed to determine the biological functions impacted by the identified DE transcripts in each subset. Interestingly, four pathways among the top 25 significant pathways (p-value <0.05) were impacted in all three cell types: *Human cytomegalovirus infection* (mcc05163), *IL-17 signaling* (mcc04657), *Viral protein interaction with cytokines and cytokine receptors* (mcc04061) and *Parathyroid hormone synthesis, secretion and action* (mcc04928) (Figures 3B and 3C). Identification of common affected pathways in all cell subsets demonstrated the substantial global impact of RhCMV on, intrinsic, innate, and adaptive immunity (40). Upregulated and downregulated genes in the first three, more closely immune-related pathways, are shown in volcano plots with pie charts used as markers for genes to indicate pathway membership (Figure 3C). Although the KEGG pathway database does not include IL-10 signaling, many of the coordinately regulated genes in different pathways are members of the Reactome IL-10 signaling pathway (shown in bold in Figure 3C). Indeed, analysis of DE genes in the Reactome pipeline demonstrates significantly differently regulation of IL-10 signaling in the APC subset (p= 0.004). Higher levels of the *IL10RA* transcript were also found in APC from RhCMV+ macaques (p_{adj}= 0.106).

Innate transcriptional profile of flow-sorted NKG2A/C$^+$ CD8$^+$ T cells

We hypothesized that expression of NKG2A/C by CD8$^+$ T cells (Figure 1F) might reflect broader up-regulation of many genes related to natural killer or other innate cells. Therefore, the transcriptional landscape and function of NKG2A/C$^+$CD8$^+$ T cells was analyzed (Supplemental Figures 6A-C for sort strategy and purity check, averaging 96.8% ± 1.4). Multidimensional scaling (MDS) was first used to place the cells within the relative transcriptional landscape of sorted subsets from RhCMV+ or RhCMV- animals (Table 1; Figure 4A). An MDS plot based on leading log2-fold changes between samples (edgeR::plotMDS function) demonstrated substantial overall similarity between NKG2A/C$^+$CD8$^+$ T cells and NK cells. In fact, NKG2A/C$^+$CD8$^+$ T cells clustered more closely to NK cells than to NKG2A/C$^-$CD8$^+$ T cells, suggesting the existence of an overall NK-like transcriptional program associated with NKG2A/C expression.

Differential gene expression analysis was then performed to identify protein-coding transcripts differentially expressed between NKG2A/C$^+$CD8$^+$ and NKG2A/C$^-$CD8$^+$ T cells from RhCMV+ animals, yielding a total of 862 DE transcripts (p_{adj}<0.05; Figure 4B). Among the significant 862 DE transcripts, as expected, *KLRC1* (NKG2A) transcripts were significantly more abundant in NKG2A/C$^+$CD8$^+$ T cells than on NKG2A/C$^-$CD8$^+$ T cells. Of note, both *KLRC2* and *KLRC3* expression (NKG2C-1 and NKG2C-2 (41)) were also abundant among NKG2A/C$^+$CD8$^+$ T cells. Increased expression of DAP-12 (*TYROBP*), a transmembrane adapter that pairs with activating NK receptors, was also detected, as was increased expression of DAP-10 (*HOPX*). Additionally, we found that numerous genes that likely enhance NK-cell responses were upregulated, including *KLRD1* (CD94), the natural cytotoxicity triggering receptors 3 and 1 (*NCR3* and *NCR1*, respectively), and cytokine receptors (e.g., *IL2RB*). Increased expression of genes related to cytolytic

effector functions, including granulysin (*GNLY*) and granzymes A and B *(GZMA* and *GZMB)*, was also seen. Gene-set enrichment analysis for members of all KEGG pathways revealed that the single most enriched pathway was *NK cell-mediated cytotoxicity* (p_{adj}< 0.01). Among the individual genes identified as DE in NKG2A/C$^+$CD8$^+$ T cells (p_{adj}<0.05), 24 were associated with this KEGG pathway (labeled in red in Figure 4B).

Innate-memory transcriptional profile and IL-15 and IL-12/IL-18 responsiveness of NKG2A/C$^+$CD8$^+$ T cells

Recently, a population of human T cells with features similar to murine virtual memory CD8$^+$ T cells (T_{VM}) was reported (20, 26). T_{VM} cells arise in the periphery, and their generation is dependent on IL-15 signaling; thus, T_{VM} express IL15Rβ (CD122 or IL2Rβ) (23). The transcriptional profile of T_{VM} cells has been reported several times and is well defined (reviewed in ref. (21)). The transcriptome of NKG2A/C$^+$CD8$^+$ T cells overlaps in many respects with the T_{VM} transcriptome, including high expression of *GNLY* as well as certain granzymes (*GZMA* and *GZMB*; Figure 4B), inflammatory cytokines (*IFNG*, *CCL5*), and cytokine receptors (*IL-2Rβ*; Figure 5A); lower expression of *CCR7* and *CCR9* (Figure 5A), which may limit the cells' retention in lymph nodes and access to the small intestine respectively; decreased expression of *SOX4*, a transcription factor for memory cell differentiation (Figure 5A); and higher expression of Eomes (Figure 5B).

Given the importance of IL-15 in stimulating mouse TVM development (23), we next tested the IL-15 responsiveness of NKG2A/C$^+$CD8$^+$ T cells *in vivo* (Figure 5C-D). Rhesus macaques were administered four doses of recombinant IL-15 (10 μg/kg) and IL-15Rα (40 μg/kg), and frequencies of T- and NK-cell subsets were followed. All treated

macaques underwent expansion of NKG2A/C^{+}CD8^{+} but not NKG2A/C^{-}CD8^{+} T cells (Table 1; Figure 5C), which was driven by increased proliferation as demonstrated by Ki-67 expression (Figure 5D). *In vitro*, similarly, after 12 days of culturing purified CD8^{+} T cells with recombinant IL-15 (50 ng/ml), a significant increase in the percentage of NKG2A/C^{+}CD8^{+} T cells was observed (Table 1; Figure 6A). NKG2A/C expression on CD8^{+} T cells increased during IL-15 culture with higher NKG2A and EOMES expression associating with increased proliferation (Figure 6B). IL-15 was able to stimulate *de novo* NKG2A/C expression after 12 days of culture of sorted NKG2A/C^{-}CD8^{+} T cells (Figure 6C). IL-15-induced NKG2A/C^{+}CD8^{+} T cells mainly exhibited a CD95^{+}CCR7^{-}CD28^{-} phenotype (Figure 6D). We next tested if NKG2A/C^{+} CD8^{+} T cells share with T_{VM} cells the ability to respond to IL-12 and IL-18 without simultaneous TCR stimulation (25, 26). Total PBMCs were cultured for 48h in the presence of IL-12 and IL-18. NKG2A/C^{+}CD8^{+} T cells responded to IL-12 and IL-18 stimulation by generating IFN-ɣ, a capacity shared with NK cells but not found among NKG2A/C^{-}CD8^{+} T cells (Table 1; Figure 6E).

Cytotoxicity of NKG2A/C^{+}CD8^{+} T cells elicited by RhCMV infection or RhCMV-vectored vaccine administration

We tested if NKG2A/C^{+}CD8^{+} T cells have NK-like killing function by analyzing their activity in the presence of MHC class I-deficient K562 target cells (Table 1; Figure 7A-B). A Calcein AM-based killing assay was used to assess cytolytic activity against K562 cells of sorted NKG2A/C^{-}CD8^{+} T cells, NKG2A/C^{+}CD8^{+} T cells, or NK cells (Figure 7A; Supplemental Figures 7A-B for sort strategy and purity checks). After sorting the average purity of NKG2A/C^{-} CD8^{+} T cells was 99.3% ± 0.4, for NKG2A/C^{+} CD8^{+} T cells was 96.3% ± 1.7 and for NK cells was 96.5% ± 0.8. NK cells and NKG2A/C^{+}CD8^{+} T cells, but not

NKG2A/C$^-$CD8$^+$ T cells, efficiently killed the targets. Furthermore, both NK cells and NKG2A/C$^+$ cells, but not NKG2A/C$^-$ cells, were stimulated to express cytokines by co-incubation with K562s (Figure 7B).

We next tested if animals receiving a RhCMV-vectored vaccine would generate substantial populations of CD8$^+$ T cells expressing NKG2 receptors, as observed in those infected by wild-type RhCMV (Figure 1F). These vaccines are based on the 68-1 strain of RhCMV strain, which lacks epithelial tropism due to the deletion of genes in the ULb' region that code for members of the pentameric virion-surface complex essential for entry to epithelial cells (9). All RhCMV-vaccinated macaques manifested expansion of NKG2A/C$^+$CD8$^+$ T cells, which in most cases reached peak frequency in the blood two weeks after vaccination (Table 1; Figure 7C). In contrast, only minor expansion of the cells was observed following administration of adenoviral vectors. Furthermore, although the vast majority of antigen-specific T cells elicited by RhCMV/SIV vaccination were NKG2A/C negative (35), viral inhibition assays showed that post-vaccination NKG2A/C$^+$ and NKG2A/C$^-$ T cells had equivalent capacity to inhibit SIV replication ex vivo (Figure 7D).

DISCUSSION

RhCMV and HCMV infections have broad impact on the infected host's immune system, which extends to phenotypic changes in nearly all subsets examined including APCs, T cells, and NK cells (3). The ubiquity of this impact is substantial, considering that active replication in immunocompetent hosts, as evidenced in plasma viremia, can be relatively brief after primary exposure (42). Another parameter of persistent infection, shedding of infectious virus in bodily fluids, can be relatively brief or intermittent when primary infection is after childhood, but shedding can persist for years when healthy immunocompetent children are infected during early childhood or *in utero* (43) .

RhCMV-seropositive and –seronegative animals in this study were housed and fed together, in outdoor corrals, minimizing the possible influence of environmental confounders on the results. Identical-twin studies have shown that the influences of non-heritable factors, such as HCMV infection, predominate over genetic influences in immunologic impact (3). Our results expand upon those previously obtained in studies of adolescent or adult, non-SPF or SPF rhesus macaques (1, 38). Previous authors demonstrated increased memory and effector $CD4^+$ and $CD8^+$ T-cell populations in non-SPF (RhCMV seropositive) compared to SPF level 2 (RhCMV seronegative) animals, including higher IL-4 production among seropositive macaques. Our findings in recently infected infants demonstrate early effects of RhCMV infection on immune homeostasis, including reduction of naïve T cells, accumulation of memory and effector cells, and capacity for production of Th2 cytokines. Thus, the effects of CMV seroconversion are established early and persist into adulthood.

Many have hypothesized that development of effector-memory cells in CMV-infected individuals is due to the location, level, or long-term persistence of antigen expression (44). Our data show that RhCMV infection has a broad transcriptional effect on T and NK cells, without an exclusive requirement for antigen responsiveness. Collins et al. recently demonstrated that a transcription factor-based scheme was evolutionarily conserved between innate and adaptive lymphocytes (45), suggesting the possibility that alterations in adaptive cells in CMV infection are not necessarily related to antigen load. Marked changes in the activation phenotype of APCs from RhCMV-infected animals suggest that an altered costimulatory environment contributes to changes seen in the T-cell compartment. Altered APC activation in young animals may also affect T-cell development within the thymus, as it has been documented in mice that CD83 is essential for thymic maturation of $CD4^+$ T cells (46-48).

Other transcriptomic associations of RhCMV infection were shared across innate and adaptive subsets. CX3CR1, a discriminative marker for HCMV-specific $CD8^+$ T cells (49), was up regulated in sorted dendritic cells, $CD8^+$NKG2A/C^- T cells and NK cells from RhCMV-infected macaques. *PTGS2,* also known as cyclooxygenase-2 (COX-2), was down regulated in all sorted populations. COX-2 is a key rate-limiting enzyme in the eicosanoid synthetic pathway for prostaglandins from arachidonic acid. The presence of a virally encoded COX-2 enzyme is a unique characteristic of RhCMV (50). Human CMV, which does not encode a viral COX-2 isoform, has been shown to induce endogenous COX-2 ("cellular" or cCOX-2) expression, and cCOX-2 activity has been shown to be essential for normal virus replication (51, 52). In rhesus macaques, expression of a virally encoded COX-2 may obviate the need for cCOX-2 induction during infection. Reduced *PTGS2* expression was seen together with decreased *IL1B*, *PTGER2*, *CCL3, CCL3L1,*

CXCL8, CDKN1A as well as increased *CCR1, TNFRSF1A, TNFRSF1B, JAK1 and CCL5*—all associated with IL-10 signaling. Both HCMV and RhCMV encode cellular IL-10 (cIL-10) orthologs (cmvIL-10 and rhcmvIL-10, respectively) that bind to IL-10R1, in each case exhibiting comparable functionality to cIL-10 (53-55). Additionally, IL-4 and cIL-10 efficiently inhibit the production of proinflammatory cytokines, such as TNF-α, IL-1α, IL-1β, IL-6, and IL-8 by monocytes/macrophages (56-58) and, indeed, we observed statistically significantly lower expression of IL-1β within sorted dendritic cells. cmvIL-10 also inhibits the expression of MHC class II and the co-stimulatory molecules CD80, CD86 and CD83 (59). Although only CD83 was shown significantly decreased at the transcript level, we observed clear downregulation of CD86 and CD83 at the protein level. IL-10RA expression was elevated in APCs from RhCMV+ macaques, which suggests that inhibitory signaling to APCs may be one mechanism by which cIL-10 regulates adaptive immunity (60).

RhCMV infection was also associated with expansion of NKG2A/C-expressing $CD8^+$ T cells, which exhibited remarkable transcriptional similarity to NK and T_{VM} cells (21). Effector functions of NKG2A/C^+CD8^+ T cells were identical to those described for T_{VM}s, including prompt IFN-ɣ production in response to innate-like stimulation by IL-12 and IL-18 (20). NKG2A/C^+CD8^+ T cells acquired NK-like cytotoxic activity against MHC class I molecule-deficient K562 cells and secreted cytokines in response to the same targets. NKG2A/C^+CD8^+ T cells were expanded in RhCMV-seronegative animals vaccinated with RhCMV 68-1-based vaccines. Remarkably, NKG2A/C^+CD8^+ T cells from vaccinated animals demonstrated comparable capacity to control SIV replication *ex vivo* to that of NKG2A/C^-CD8^+ T cells, despite the fact that few NKG2A/C^+CD8^+ are specific for vaccine epitopes (35).

IL-15 is mainly produced by monocytes/macrophages and dendritic cells (61). Type-I IFNs, production of which is induced by infections such as RhCMV, can regulate IL-15 signaling by causing such antigen-presenting cells to increase the amount of IL-15 available (62). It has been also reported that type-I IFN signaling can increase sensitivity of $CD8^+$ T cells to IL-15 by increasing expression of Eomes, a T-box transcription factor that promotes expression of IL-2Rβ (63).

IL-15 is known critical for T_{VM} generation (23) and was shown in this work to be capable of inducing *de novo* NKG2A/C expression on purified $NKG2A^-CD8^+$ T cells (Figure 6C). In previous studies, Correia et al. (64, 65) showed that IL-15 could induce KIR, NKG2A and NKp46 on peripheral blood $CD8^+$ T cells. $NKG2A/C^+CD8^+$ T cells from RhCMV-infected macaques express high levels of the *IL2Rβ* transcript, whose protein product is required for IL-15 signaling. These cells also express elevated levels of the *IL15RA* transcript ($p=0.026$) and similar levels of the *IL2RG* transcript compared to $NKG2A/C^-CD8^+$ T cells. Indeed, we observed a substantial expansion and proliferation of $NKG2A/C^+CD8^+$ T cells following recombinant IL-15/IL-15Rα administration, which was greater than observed for conventional, NKG2A/C-negative CD8 T cells. Although the small sample size of our interventional experiment is a limitation, the expansion we observed fits neatly with similar expansion of NK cells, known to be IL-15 responsive, after HCMV infection.

Furthermore, Langerhans cells, which are the most abundant innate immune cells at oral and genital mucosae, natural routes of HCMV acquisition (66), can secrete more IL-15 than other conventional DC subtypes (67), and induce $CD8^+$ naïve T cells to express NK-associated markers and acquire antimicrobial activity. The resulting antimicrobial CTLs

(amCTLs) are associated with protection against *Mycobacterium tuberculosis* (68) and *Mycobacterium leprae* (27). The possibility that CMV-induced NKG2A/C-expressing T cells are functionally similar to amCTLs suggests a mechanism for the promising efficacy of CMV-based vaccines against *M. tuberculosis* (36).

Thus, expansion of innate-like $CD8^+$ T cells following RhCMV infection or vaccination is driven largely by host IL-15 expression and associated with invocation of an NK- and T_{VM}-like transcriptional program, as well as acquisition of T_{VM}-like effector functions. NKG2A/C^+CD8^+ T cells are able to kill NK-cell targets (K562), suggesting that the NK-associated receptors expressed on NKG2A/C^+CD8^+ T cells have similar functional implications for the expressing cell. Furthermore, NKG2A/C^+CD8^+ T cells were observed to expand after RhCMV 68-1/SIV vaccination and have the potential to control SIV replication *ex vivo*. A recent report supports the association of RhCMV/SIV vaccine-mediated protection with IL-15 signaling (69). We conclude that NKG2A/C^+CD8^+ T cells are innate-memory cells of macaques, whose expansion is driven by IL-15 and which may contribute to control over viral infections (26, 70, 71).

MATERIAL AND METHODS

Study design

The survey of infant macaques was an observational study aimed at identifying immunologic changes in cells of the circulating immune system associated with RhCMV infection. Specifically, we hypothesized between-group differences in the frequency of (i) innate immune cells with adaptive features, such as g-NK cells, and (ii) adaptive immune cells with innate features, such as NK-CTL. Healthy, genetically outbred rhesus macaques (*Macaca mulatta*) from the California National Primate Research Center (CNPRC), tested twice and confirmed to be either RhCMV seronegative (RhCMV) or RhCMV seropositive (RhCMV+), were used for immunophenotyping studies and transcriptomic analysis. Both RhCMV- and RhCMV+ animals were born, reared, and co-housed in outdoor corrals at the CNPRC and were exposed to same diet and environment. The sample included all animals of the correct age and housing situation. The vaccine study used outbred rhesus macaques from the SPF level 2 colony at the CNPRC, which is maintained free of CMV, randomized to vaccination with adenovector or RhCMV. Conventional SPF level 1 rhesus macaques (RhCMV+) were used for IL-15 and IL-15Rα *in vivo* administration study and *in vitro* functional responsiveness studies. Sample sizes for the latter two studies were based upon likelihood of SIV control and of cytokine-driven T-cell proliferation, respectively, which were most relevant to the pre-specified hypotheses. Conventional RhCMV+ macaques were randomly selected and used for *in-vitro* functional responsiveness studies. Blood samples were taken from each rhesus macaque for plasma and PBMCs. Plasma samples were stored at -70˚C. PBMCs were isolated by gradient density purification using Lymphocyte Separation Medium (MP Biomedicals, LLC).

Immune cell phenotyping by flow cytometry

Naïve/memory/effector T cell composition, T cell activation, T_{reg}, NK cells and APC were evaluated using fresh unstimulated rhesus macaque PBMCs stained with predetermined optimal concentrations of the following antibodies: anti-CD3–Alexa 700 (clone SP34-2) (Cat# 557917, BD Biosciences), anti-CD3–Pacific Blue (clone SP34-2) (Cat# 558124, BD Biosciences), anti-CD95–APC (clone DX2) (Cat# 558814, BD Biosciences), anti-CD95–FITC (clone DX2) (Cat# 555673, BD Biosciences), anti-CD28–APC-H7 (clone CD28.2) (Cat# 561368, BD Biosciences), anti-CCR5–APC (clone 3A9) (Cat# 550856, BD Biosciences), anti-Ki67–Alexa 488 (clone B56) (Cat# 561165, BD Biosciences), anti-CD127–PE (clone HIL-7R-M21) (Cat# 557938, BD Biosciences), anti-CD25–PE-Cy7 (clone M-A251) (Cat# 557741, BD Biosciences), anti-CD123–peridinin chlorophyll protein–Cy5.5 (clone 7G3) (Cat# 558714, BD Biosciences), anti–HLA-DR–PE-Cy7 (clone L243) (Cat# 335795, BD Biosciences), anti-CD16–PacBlue (clone 3G8) (Cat# 558122, BD Biosciences), anti-CD83–PE (clone HB15e) (Cat# 550634, BD Biosciences), anti-CD80–FITC (clone L307.4) (Cat# 557226, BD Biosciences), anti-CD86–APC (clone 2331 (FUN-1)) (Cat# 555660, BD Biosciences), anti-CD56–AF700 (clone B159) (Cat# 557919, BD Biosciences), anti-CD8–PE-Cy5.5 (clone 3B5) (Cat# MHCD0818, Thermo Fisher Scientific), anti-CD14–Qdot 605 (clone TUK4) (Cat# Q10013, Thermo Fisher Scientific), anti–CD20 PE-Texas Red (clone HI47) (Cat# MHCD2017, Thermo Fisher Scientific), LIVE/DEAD™ Fixable Aqua Dead Cell Stain Kit (Cat# L34966, Thermo Fisher Scientific), anti-CD11c–Alexa 700 (clone 3.9) (Cat# 56-0116-42, Thermo Fisher Scientific), anti-FOXP3–PacBlue (clone 206D) (Cat# 320116, BioLegend), anti-CD28–Alexa 700 (clone CD28.2) (Cat# 302920, BioLegend), anti-CD4–Qdot 655 (19Thy5D7) (Cat# PR-4190, NIH Nonhuman Primate Reagent Resource), anti-CD38–PE (clone OKT10) (Cat# PR-

3802, NIH Nonhuman Primate Reagent Resource), and anti–HLA-DR–ECD (clone Immu-357) (Cat# IM3636, Beckman Coulter), anti–CD45RA–ECD (clone 2H4) (Cat# IM2711U, Beckman Coulter), anti-CD159a–PECy7 (clone z199) (Cat# B10246, Beckman Coulter). FOXP3 Fix/Perm kit (Cat# 421403, BioLegend) was used to intranuclearly stain with anti-FOXP3 and anti-Ki67, washed, fixed in phosphate-buffered saline containing 1% paraformaldehyde, and acquired on a BD Fortessa cytometer. Analysis was performed using FlowJo version 10.3.

Cytokine flow cytometry assay

Levels of cytokine-producing cells were determined by cytokine flow cytometry after stimulation with phorbol 12-myristate 13-acetate (PMA) and ionomycin. Rhesus macaque PBMCs were resuspended to 10^6 cells/ml in RPMI 1640 supplemented with 10% FBS and penicillin/streptomycin (cRPMI). Cells were then incubated for 6 hours at 37°C in medium containing PMA (50 ng/ml) (Sigma-Aldrich), ionomycin (1 µg/ml) (Sigma-Aldrich), and Brefeldin A (5 µg/ml) (Biolegend). After incubation, cells were washed and stained with surface LIVE/DEAD™ Fixable Aqua Dead Cell Stain Kit (Cat# L34966, Thermo Fisher Scientific), anti-CD8–PE-Cy5.5 (clone 3B5) (Cat# MHCD0818, Thermo Fisher Scientific), anti-CD4–Qdot 655 (19Thy5D7) (Cat# PR-4190, NIH Nonhuman Primate Reagent Resource, anti-CD3–Pacific Blue (clone SP34-2) (Cat# 558124, BD Biosciences), anti-CD95–APC (clone DX2) (Cat# 558814, BD Biosciences) and anti-CD28–APC-H7 (clone CD28.2) (Cat# 561368, BD Biosciences). Cells were then washed, permeabilized using a Cytofix/Cytoperm kit (Cat# 554714, BD Biosciences) according to the manufacturer's instructions, intracellularly stained with anti-IL-17–PE (clone eBio64CAP17) (Cat# 12-7178-42, Thermo Fisher Scientific), anti-IL-4 FITC (clone MP4-

25D2) (Cat# 500806, BioLegend), anti-IFN-γ–PE-Cy7 (clone B27) (Cat# 557643, BD Biosciences) and anti-TNFα Alexa 700 (clone Mab11) (Cat# 557996, BD Biosciences), washed, fixed in phosphate-buffered saline containing 1% paraformaldehyde, and acquired on a BD Fortessa cytometer. Analysis was performed using FlowJo version 10.3.

3' RNA tag sequencing

PBMCs from six RhCMV+ and six RhCMV- rhesus macaques were stained with surface markers anti-CD3–Pacific Blue (clone SP34-2) (Cat# 558124, BD Biosciences), anti-CD4–APC (clone L200) (Cat# 551980, BD Biosciences), anti-CD8–AF700 (clone RPA-T8) (Cat# 561453, BD Biosciences), anti-CD20–FITC (clone L27) (Cat# 347673, BD Biosciences), anti-CD11c–PE (clone 3.9) (Cat# 301606, BioLegend) and anti-CD159a–PECy7 (clone z199) (Cat# B10246, Beckman Coulter); sorted on FACS Aria (BD Biosciences) into four subpopulations with the following profiles; $CD3^-CD20^-HLADR^+CD11c^+$ ($CD11c^+$ DC), $CD3^+CD20^-CD8^+NKG2A/C^+$ ($NKG2A/C^+$ $CD8^+$ T cells), $CD3^+CD20^-CD8^+NKG2A/C^-$ ($NKG2A/C^-$ $CD8^+$ T cells) and $CD3^-CD20^-CD8^+NKG2A/C^+$ (NK cells) and used for RNA-seq analysis. Sorted cells with the profiles given above were resuspended in RNAlater and stored at -70°C until RNA extraction. Total RNA was extracted from these sorted cells using the Total RNA Purification Micro Kit (Norgen Biotek Corp) according to manufacturer's protocol. The quantity and quality of total RNA extracted was checked using the Nanodrop 2000 (ThermoFisher Scientific) and the Agilent 2100 Bioanalyzer (Agilent Technologies). Libraries were prepared by the UC Davis DNA Technologies Core using the Quant Seq kit (Lexogen Inc.) following the manufacturer's protocol for 3' mRNA-sequencing. Libraries were pooled and sequenced

using the Illumina HiSeq 4000 (Illumina) with 90-bp, single-ended stranded sequencing. Sequence quality was checked using fastqc (75) and aligned to Macaca mulatta genome assembly version Mmul_10 annotated with Macaca_mulatta.Mmul_10.99.gtf using STAR (76) to generate a matrix of feature counts. Differential gene expression was analyzed using the R package *edgeR* (77). Read counts were normalized using the TMM method. Prior to analysis, low-variability genes (defined here as having less than 10 normalized reads in all samples) were filtered, leaving 10,596 genes. Differential expression analyses were conducted using the limma-voom Bioconductor pipeline, using a model with factors for marker-RhCMV status interaction and fragmentation time. Standard errors of estimates were adjusted for within-animal correlation. Differentially expressed genes were defined to have an adjusted p-value less than 0.05.

Recombinant IL-15 and IL-15Rα in vivo administration

Starting from day 0, three animals were treated with 4 weekly doses (subcutaneous) of recombinant IL-15 (10ug/Kg) and IL-15Rα-Fc (40ug/Kg). Peripheral blood sample collections were performed on the day of administration of each dose, 3 and 7 days after each dose and PBMCs were cryopreserved. Frozen PBMCs were stained with surface markers LIVE/DEAD™ Fixable Aqua Dead Cell Stain Kit (Cat# L34966, Thermo Fisher Scientific), anti-CD3–APC-Cy7 (clone SP34-2) (Cat# 557757, BD Biosciences), anti CD8–PerCP-Cy5.5 (clone SK1) (Cat# 341049, BD Biosciences) and anti-CD159a–PE (clone z199) (Cat# IM3291U, Beckman Coulter). Cells were then washed, permeabilized using a Cytofix/Cytoperm kit (BD Biosciences) according to the manufacturer's instructions, intracellularly stained with anti-Ki67–Alexa 488 (clone B56) (Cat# 561165, BD Biosciences), washed, fixed in phosphate-buffered saline containing 1%

paraformaldehyde, and acquired on a BD Fortessa cytometer. Analysis was performed using FlowJo version 10.3.

Cytokine production and cytotoxicity assay

For the cytokine production assay, PBMCs were stimulated with target tumor cells (K562, source CNPRC) at a ratio of 10:1 (E:T) in cRPMI for 6 hours at 37°C in the presence of Brefeldin A (Biolegend) or with rhesus rIL-12 and rIL18 (20ng/ml or 50ng/ml, each) from R&D Systems™ for 44h at 37°C followed by 4h of stimulation in the presence of Brefeldin A (Biolegend). After incubation, cells stimulated with K562 were washed and stained with surface markers LIVE/DEAD™ Fixable Aqua Dead Cell Stain Kit (Cat# L34966, Thermo Fisher Scientific), anti-CD3–Alexa 700 (clone SP34-2) (Cat# 557917, BD Biosciences), anti-CD20–APC-H7 (clone 2H7) (Cat# 560734, BD Biosciences), anti-CD159a–PE-Vio770 (clone REA110) (Cat# 130-105-694, Miltenyi Biotec), anti-CD8–Pacific Blue (clone SK1) (Cat# 740093, BD Biosciences). Cells were then washed, permeabilized using a Cytofix/Cytoperm kit (BD Biosciences) according to the manufacturer's instructions, intracellularly stained with anti-IFN-γ–APC (clone B27) (Cat# 554702, BD Biosciences) and anti-TNFα–PE (clone Mab11) (Cat# 554513, BD Biosciences), washed, fixed in phosphate-buffered saline containing 1% paraformaldehyde, and acquired on a BD Fortessa cytometer. Analysis was performed using FlowJo version 10.3.

After 48 hours incubation, cells stimulated with rhesus rIL-12 and rIL18 were washed and stained with surface markers LIVE/DEAD™ Fixable Aqua Dead Cell Stain Kit (Cat# L34966, Thermo Fisher Scientific), anti-CD8–PerCP-Cy™5.5 (clone SK1) (Cat# 341049, BD Biosciences), anti-CD3–BUV737 (clone SP34-2) (Cat# 741872, BD Biosciences), anti-CD4–BV650 (clone L200) (Cat# 563737, BD Biosciences) and anti-CD159a

(NKG2A)–VioBright FITC (clone REA110) (Cat# 130-113-568, Miltenyi Biotec). Cells were then washed, permeabilized using a Cytofix/Cytoperm kit (BD Biosciences) according to the manufacturer's instructions, intracellularly stained with anti-IFN-γ–PE-Cy7 (clone B27) (Cat# 557643, BD Biosciences), washed, fixed in phosphate-buffered saline containing 1% paraformaldehyde, and acquired on a BD FACSymphony™ Flow Cytometer. Analysis was performed using FlowJo version 10.3.

For the cytotoxicity assay, PBMCs were stained with surface markers anti-CD3–Pacific Blue (clone SP34-2) (Cat# 558124, BD Biosciences), anti-CD4–BV605 (Clone L200) (Cat# 562843, BD Biosciences), anti-CD8–AF700 (clone RPA-T8) (Cat# 561453, BD Biosciences) and anti-CD159a–PECy7 (clone z199) (Cat# B10246, Beckman Coulter); sorted on FACS Aria (BD Biosciences) into three subpopulations with the following profiles; $CD3^+CD8^+NKG2A/C^+$ ($NKG2A/C^+$ $CD8^+$ T cells), $CD3^+CD8^+NKG2A/C^-$ ($NKG2A/C^-$ $CD8^+$ T cells) and $CD3^-CD8^+NKG2A^+$ (NK cells). Sorted cells were incubated in cRMPI with K562 tumor cells stained with 2μM calcein AM (BD Biosciences) at a ratio of 5:1 (E:T) in a 96-well U-bottom plate for 4 hours. Supernatant were collected from wells containing both effector and target cells (specific lysis), wells containing only target cells (spontaneous lysis), and wells containing target cells lysed with 0.1% Tween-20 (total lysis), and fluorescence were measured at 495/515 nm. The percentage of specific lysis was calculated using the measured fluorescence as follow: 100 x (specific lysis – spontaneous lysis) / (total lysis – spontaneous lysis).

Recombinant IL-15-induced NKG2A expression assay

$CD8^+$ T cells were purified from PBMCs using magnetically activated cell sorting (MACS) nonhuman primate CD8 MicroBead kit (Miltenyi Biotec) according to the manufacturer's instructions or sorted on FACS Aria (BD Biosciences) into $CD3^+CD8^+NKG2A/C^-$ ($NKG2A/C^-$ $CD8^+$ T cells) and cultured for 12 days with recombinant IL-15 (50ng/ml). After incubation, cells were washed and stained with surface markers for LIVE/DEAD™ Fixable Aqua Dead Cell Stain Kit (Cat# L34966, Invitrogen), anti-CD3–Pacific Blue (clone SP34-2) (Cat# 558124, BD Biosciences), anti-CD4–BV605 (Clone L200) (Cat# 562843, BD Biosciences), anti-CD8–FITC (clone SK1) (Cat# 344704, Biolegend), anti-CD159a–PE-Cy7 (clone z199) (Cat# B10246, Beckman Coulter), anti-CD95–APC (clone DX2) (Cat# 558814, BD Biosciences), anti-CD28–APC-H7 (clone CD28.2) (Cat# 561368, BD Biosciences) and anti-CCR7–BV786 (clone 3D12) (Cat# 563710, BD Biosciences). For proliferation studies purified $CD8^+$ T cells were isolated using magnetically activated cell sorting (MACS) nonhuman primate CD8 MicroBead kit (Miltenyi Biotec) according to the manufacturer's instructions and labeled with 2.5μM CFSE (Invitrogen). After incubation for 12 days in the presence of recombinant IL-15 (50ng/ml) cells were washed and stained with surface markers for LIVE/DEAD™ Fixable Far Red Dead Cell Stain Kit (Cat# L34973, Invitrogen), anti-CD3–Pacific Blue (clone SP34-2) (Cat# 558124, BD Biosciences), anti-CD4–BV605 (clone L200) (Cat# 562843, BD Biosciences), anti-CD8–BUV805 (clone SK1) (Cat# 612890, BD Biosciences) and anti-CD159a–PE-Cy7 (clone z199) (Cat# B10246, Beckman Coulter). Cells were then washed, permeabilized using BD Pharmingen™ Transcription Factor Buffer Set according to the manufacturer's instructions, intranuclearly stained with anti-EOMES–efluor660 (Cat# 50-4877-42, Thermo Fisher Scientific), washed, fixed in phosphate-buffered saline containing 1%

paraformaldehyde, and acquired on a BD FACSymphony™ Flow Cytometer. Analysis was performed using FlowJo version 10.3.

Vaccine administration

Starting from day 0, six and eight SPF level 2 (RhCMV seronegative) animals received either an Adenoviral-vectored or a RhCMV-vectored vaccine prime and a booster on day 28 after priming. Whole blood samples were collected on the day of vaccination, and 3, 7, 14 and 28 days after vaccine prime and vaccine boost. Surface staining with markers anti-CD3–BUV737 (clone SP34-2) (Cat# 741872, BD Biosciences), anti-CD4–BUV395 (clone L200) (Cat# 564107, BD Biosciences), anti-CD8–BUV805 (clone SK1) (Cat# 612890, BD Biosciences) and anti-CD159a (NKG2A)–VioBright FITC (clone REA110) (Cat# 130-113-568, Miltenyi Biotec) was performed for 50 µl whole blood samples. Q-Prep was used according to the manufacturer's recommended protocol that was provided in the product insert (Beckman Coulter, Inc.) and acquired on a BD FACSymphony™ Flow Cytometer.

Virus inhibition assay.

Virus-inhibitory activity (VIA) was measured as follows. PBMC targets were depleted of $CD8^+$ cells using a magnetically activated cell sorting (MACS) nonhuman primate CD8 MicroBead kit (Miltenyi Biotec) according to the manufacturer's instructions. Targets were then resuspended in cRPMI and stimulated with PHA (5 µg/ml) in the presence of recombinant human interleukin-2 (rhIL-2) at a concentration of 20 U/ml (Miltenyi Biotec). After stimulation for two days, the medium was replenished and target PBMCs were infected at 1-3 × 10^6 cells/ml using a SIVmac251 stock at a multiplicity of infection (MOI)

of 0.01 for one day at 37°C and 5% CO2. Following infection, cells were resuspended and plated at 5 × 10^4 cells per well in a U-bottom, 96-well tissue culture plate. The same day PBMCs stained with surface markers anti-CD3–Pacific Blue (clone SP34-2) (Cat# 558124, BD Biosciences), anti-CD4–BV605 (clone L200) (Cat# 562843, BD Biosciences), anti-CD8–FITC (clone SK1) (Cat# 344704, Biolegend) and anti-CD159a–PECy7 (clone z199) (Cat# B10246, Beckman Coulter) were sorted into three subpopulations with the following profiles; $CD3^+CD8^+NKG2A/C^+$ (NKG2A/C$^+$ CD8$^+$ T cells), $CD3^+CD8^+NKG2A/C^-$ (NKG2A/C$^-$ CD8$^+$ T cells) and $CD3^-CD8^+NKG2A^+$ (NK cells). Effector cells, sorted as described above, were diluted and added to autologous infected targets at an effector/target (E:T) ratio of 1:1. Infectivity controls consisted of infected targets without added effectors. Duplicate co-cultures were incubated at 37°C and 5% CO2 for six days. After incubation, cells were washed and stained with surface markers for LIVE/DEAD™ Fixable Aqua Dead Cell Stain Kit (Cat# L34966, Invitrogen), anti-CD3–Pacific Blue (clone SP34-2) (Cat# 558124, BD Biosciences), anti-CD4–BV605 (clone L200) (Cat# 562843, BD Biosciences) and anti-CD8–FITC (clone SK1) (Cat# 344704, Biolegend). Cells were then washed, permeabilized using a Cytofix/Cytoperm kit (BD Biosciences) according to the manufacturer's instructions, intracellularly stained with anti-SIV Gag p27 (clone 55-2F12) (Cat# 1610, NIH AIDS Research Reagent Program) biotin-conjugated using the One-Step Antibody Biotinylation Kit (Miltenyi Biotec), washed and stained with APC-streptavidin (Cat# 554067, BD Biosciences), washed, fixed in phosphate-buffered saline containing 1% paraformaldehyde, and acquired on a BD FACSymphony™ Flow Cytometer. The percentage of viral inhibition was calculated using the following formula: 100 X (Fraction of $p27^+$ cells among $CD4^+$ T cells cultured alone) -

(Fraction of $p27^+$ cells among $CD4^+$ T cells cultured with effector cells) / (Fraction of $p27^+$ cells among $CD4^+$ T cells cultured alone).

Statistical analysis

R was used for all statistical analysis, and all plots were created using the *ggplot2* package (72). Wilcoxon rank-sum tests were used for comparisons of immune phenotypes by RhCMV status. Wilcoxon signed-rank test were used for comparisons in paired observations as indicated in figure legends. Friedman tests were used for comparisons of repeated measured observations, such as those in panel 7C. For all statistical tests, differences between groups were considered significant when the P value was <0.05. Principal component analysis was performed using the *ade4* package (73). The function *adonis* from the R package, *Vegan* (74), was used to assess correlations between dissimilarity of samples and factors such as CMV infection. Heatmaps were generated in R using the *heatmap2* package.

Study approval

The UC Davis animal care program is accredited by the Association for the Assessment and Accreditation of Laboratory Animal Care, International (AAALAC). All animal procedures were approved prior to implementation by the UC Davis Institutional Animal Care and Use Committee and were consistent with the requirements of the Animal Welfare Act. Activities related to animal care were performed as per standard operating procedures at the California National Primate Research Center.

Author Contributions: GML, SK, CB, PAL, PAB, and DJHO designed research studies. GML, WLWC, JL, HTK, WL, and LA. conducted experiments and performed data acquisition. GML, WLWC, NC, DM and JL analyzed the data and prepared figures and publication materials. MRU provided advice for VIA measurement and analysis. GML wrote the manuscript.

Acknowledgments: We thank Dr. Lewis Lanier for insightful comments on the manuscript. We thank the veterinary, Colony Research Clinical Laboratories, and Pathology faculty and staff at CNPRC for expert technical assistance. The authors also thank Dr. Francois Villinger for provision of recombinant Mamu IL-15 and Mamu IL-15-Rα-Fc. The following reagents were obtained through the NIH AIDS Reagent Program, Division of AIDS, NIAID, NIH: anti-SIVmac p27 monoclonal (55-2F12), Mouse Anti-Human CD4 Qdot 655 (19Thy5D7) and Mouse Anti-Human CD38 PE (clone OKT10). The sequencing was carried by the DNA Technologies and Expression Analysis Core at the UC Davis Genome Center, supported by NIH Shared Instrumentation Grant 1S10OD010786-01.

Declaration of interest: No potential conflict of interest was reported by the authors

Data Availability Statement: The expression data generated by RNA-seq analysis are available in the GEO repository under accession number GSE171978.

Funding: This work was supported by National Institutes of Health grants AI 118451 (DJHOC), AI 143554 (DJHOC and PAB), AI 131568 (DJHOC, PAB and CB), OD P51 OD011107 (California National Primate Research Center), by the California HIV/AIDS Research Foundation under award F13-D-312 to GML and by the UCSF-Gladstone Institute for Virology and Immunology, Center for AIDS Research (CFAR) under award 4P30AI027763-25 to GML.

REFERENCES

1. Santos Rocha C, Hirao LA, Weber MG, Méndez-Lagares G, Chang WLW, Jiang G, et al. Subclinical Cytomegalovirus Infection Is Associated with Altered Host Immunity, Gut Microbiota, and Vaccine Responses. *Journal of Virology.* 2018;92(13).
2. Nakaya HI, Hagan T, Duraisingham SS, Lee EK, Kwissa M, Rouphael N, et al. Systems Analysis of Immunity to Influenza Vaccination across Multiple Years and in Diverse Populations Reveals Shared Molecular Signatures. *Immunity.* 2015;43(6):1186-98.
3. Brodin P, Jojic V, Gao T, Bhattacharya S, Angel CJ, Furman D, et al. Variation in the human immune system is largely driven by non-heritable influences. *Cell.* 2015;160(1-2):37-47.
4. Ardeshir A, Narayan NR, Mendez-Lagares G, Lu D, Rauch M, Huang Y, et al. Breast-fed and bottle-fed infant rhesus macaques develop distinct gut microbiotas and immune systems. *Sci Transl Med.* 2014;6(252):252ra120.
5. Narayan NR, Mendez-Lagares G, Ardeshir A, Lu D, Van Rompay KK, and Hartigan-O'Connor DJ. Persistent effects of early infant diet and associated microbiota on the juvenile immune system. *Gut Microbes.* 2015;6(4):284-9.
6. Ivanov, II, Atarashi K, Manel N, Brodie EL, Shima T, Karaoz U, et al. Induction of intestinal Th17 cells by segmented filamentous bacteria. *Cell.* 2009;139(3):485-98.
7. De Vlaminck I, Khush KK, Strehl C, Kohli B, Neff NF, Okamoto J, et al. Temporal Response of the Human Virome to Immunosuppression and Antiviral Therapy. *Cell.* 2013;155(5):1178-87.
8. Zuhair M, Smit GSA, Wallis G, Jabbar F, Smith C, Devleesschauwer B, et al. Estimation of the worldwide seroprevalence of cytomegalovirus: A systematic review and meta-analysis. *Reviews in Medical Virology.* 2019;29(3):e2034.
9. Barry PA, Deere JD, Yue Y, Chang WWL, Schmidt KA, Wussow F, et al. Cytomegalovirus-vectored vaccines for HIV and other pathogens. *AIDS (London, England).* 2020;34(3):335-49.
10. Wang A, Ren L, Abenes G, and Hai R. Genome sequence divergences and functional variations in human cytomegalovirus strains. *FEMS Immunology & Medical Microbiology.* 2009;55(1):23-33.
11. Sylwester AW, Mitchell BL, Edgar JB, Taormina C, Pelte C, Ruchti F, et al. Broadly targeted human cytomegalovirus-specific CD4(+) and CD8(+) T cells dominate the memory compartments of exposed subjects. *The Journal of Experimental Medicine.* 2005;202(5):673-85.
12. Zhang T, Scott JM, Hwang I, and Kim S. Antibody-dependent memory-like NK cells distinguished by FcRγ-deficiency(). *Journal of immunology (Baltimore, Md : 1950).* 2013;190(4):1402-6.
13. Cristina Mingari M, Vitale C, Cambiaggi A, Schiavetti F, Melioli G, Ferrini S, et al. *Cytolytic T lymphocytes displaying natural killer (NK)-like activity: Expression of NK-related functional receptors for HLA class I molecules (p58 and CD94) and inhibitory effect on the TCR-mediated target cell lysis or lymphokine production.* 1995.
14. Pietra G, Romagnani C, Falco M, Vitale M, Castriconi R, Pende D, et al. The analysis of the natural killer-like activity of human cytolytic T lymphocytes revealed HLA-E as a novel target for TCR α/β-mediated recognition. *European Journal of Immunology.* 2001;31(12):3687-93.
15. Romagnani C, Pietra G, Falco M, Millo E, Mazzarino P, Biassoni R, et al. Identification of HLA-E-specific alloreactive T lymphocytes: A cell subset that undergoes preferential expansion in mixed lymphocyte culture and displays a broad cytolytic activity against allogeneic cells. *Proceedings of the National Academy of Sciences of the United States of America.* 2002;99(17):11328-33.

16. Moretta L, Romagnani C, Pietra G, Moretta A, and Mingari MC. NK-CTLs, a novel HLA-E-restricted T-cell subset. *Trends in Immunology.* 2003;24(3):136-43.
17. Mazzarino P, Pietra G, Vacca P, Falco M, Colau D, Coulie P, et al. Identification of effector-memory CMV-specific T lymphocytes that kill CMV-infected target cells in an HLA-E-restricted fashion. *European Journal of Immunology.* 2005;35(11):3240-7.
18. Björkström NK, Béziat V, Cichocki F, Liu LL, Levine J, Larsson S, et al. CD8 T cells express randomly selected KIRs with distinct specificities compared with NK cells. *Blood.* 2012;120(17):3455-65.
19. van der Veken LT, Diez Campelo M, van der Hoorn MAWG, Hagedoorn RS, van Egmond HME, van Bergen J, et al. Functional Analysis of Killer Ig-Like Receptor-Expressing Cytomegalovirus-Specific CD8⁺ T Cells. *The Journal of Immunology.* 2009;182(1):92-101.
20. Jacomet F, Cayssials E, Basbous S, Levescot A, Piccirilli N, Desmier D, et al. Evidence for eomesodermin-expressing innate-like CD8+ KIR/NKG2A+ T cells in human adults and cord blood samples. *European Journal of Immunology.* 2015;45(7):1926-33.
21. Hussain T, and Quinn KM. Similar but different: virtual memory CD8 T cells as a memory-like cell population. *Immunology & Cell Biology.* 2019;97(7):675-84.
22. Jin J-H, Huang H-H, Zhou M-J, Li J, Hu W, Huang L, et al. Virtual memory CD8+ T cells restrain the viral reservoir in HIV-1-infected patients with antiretroviral therapy through derepressing KIR-mediated inhibition. *Cell Mol Immunol.* 2020.
23. Sosinowski T, White JT, Cross EW, Haluszczak C, Marrack P, Gapin L, et al. CD8α⁺ Dendritic Cell Trans Presentation of IL-15 to Naive CD8⁺ T Cells Produces Antigen-Inexperienced T Cells in the Periphery with Memory Phenotype and Function. *The Journal of Immunology.* 2013;190(5):1936-47.
24. Intlekofer AM, Takemoto N, Wherry EJ, Longworth SA, Northrup JT, Palanivel VR, et al. Effector and memory CD8+ T cell fate coupled by T-bet and eomesodermin. *Nature Immunology.* 2005;6(12):1236-44.
25. Lee J-Y, Hamilton SE, Akue AD, Hogquist KA, and Jameson SC. Virtual memory CD8 T cells display unique functional properties. *Proceedings of the National Academy of Sciences.* 2013;110(33):13498-503.
26. White JT, Cross EW, Burchill MA, Danhorn T, McCarter MD, Rosen HR, et al. Virtual memory T cells develop and mediate bystander protective immunity in an IL-15-dependent manner. *Nature communications.* 2016;7:11291.
27. Balin SJ, Pellegrini M, Klechevsky E, Won ST, Weiss DI, Choi AW, et al. Human antimicrobial cytotoxic T lymphocytes, defined by NK receptors and antimicrobial proteins, kill intracellular bacteria. *Sci Immunol.* 2018;3(26):eaat7668.
28. Burwitz BJ, Malouli D, Bimber BN, Reed JS, Ventura AB, Hancock MH, et al. Cross-Species Rhesus Cytomegalovirus Infection of Cynomolgus Macaques. *PLoS Pathog.* 2016;12(11):e1006014-e.
29. Hansen SG, Piatak M, Ventura AB, Hughes CM, Gilbride RM, Ford JC, et al. Immune clearance of highly pathogenic SIV infection. *Nature.* 2013;502(7469):100-4.
30. Hansen SG, Vieville C, Whizin N, Coyne-Johnson L, Siess DC, Drummond DD, et al. Effector-memory T cell responses are associated with protection of rhesus monkeys from mucosal SIV challenge. *Nature medicine.* 2009;15(3):293-9.
31. Hansen SG, Ford JC, Lewis MS, Ventura AB, Hughes CM, Coyne-Johnson L, et al. Profound early control of highly pathogenic SIV by an effector-memory T cell vaccine. *Nature.* 2011;473(7348):523-7.
32. Hansen SG, Marshall EE, Malouli D, Ventura AB, Hughes CM, Ainslie E, et al. A live-attenuated RhCMV/SIV vaccine shows long-term efficacy against heterologous SIV challenge. *Science Translational Medicine.* 2019;11(501):eaaw2607.

33. Marshall EE, Malouli D, Hansen SG, Gilbride RM, Hughes CM, Ventura AB, et al. Enhancing safety of cytomegalovirus-based vaccine vectors by engaging host intrinsic immunity. *Science Translational Medicine.* 2019;11(501):eaaw2603.
34. Gupta RK, Abdul-Jawad S, McCoy LE, Mok HP, Peppa D, Salgado M, et al. HIV-1 remission following CCR5Δ32/Δ32 haematopoietic stem-cell transplantation. *Nature.* 2019;568(7751):244-8.
35. Hansen SG, Wu HL, Burwitz BJ, Hughes CM, Hammond KB, Ventura AB, et al. Broadly targeted $CD8^+$ T cell responses restricted by major histocompatibility complex E. *Science.* 2016;351(6274):714-20.
36. Hansen SG, Zak DE, Xu G, Ford JC, Marshall EE, Malouli D, et al. Prevention of tuberculosis in rhesus macaques by a cytomegalovirus-based vaccine. *Nature medicine.* 2018;24(2):130-43.
37. Vogel P, Weigler BJ, Kerr H, Hendrickx AG, and Barry PA. Seroepidemiologic studies of cytomegalovirus infection in a breeding population of rhesus macaques. *Laboratory animal science.* 1994;44(1):25-30.
38. Oxford KL, dela Pena-Ponce MGA, Jensen K, Eberhardt MK, Spinner A, Van Rompay KKA, et al. The interplay between immune maturation, age, chronic viral infection and environment. *Immunity & Ageing : I & A.* 2015;12:3.
39. Ram DR, Manickam C, Hueber B, Itell HL, Permar SR, Varner V, et al. Tracking KLRC2 (NKG2C)+ memory-like NK cells in SIV+ and rhCMV+ rhesus macaques. *PLoS Pathog.* 2018;14(5):e1007104.
40. Wills MR, Poole E, Lau B, Krishna B, and Sinclair JH. The immunology of human cytomegalovirus latency: could latent infection be cleared by novel immunotherapeutic strategies? *Cell Mol Immunol.* 2015;12(2):128-38.
41. Walter L, and Petersen B. Diversification of both KIR and NKG2 natural killer cell receptor genes in macaques - implications for highly complex MHC-dependent regulation of natural killer cells. *Immunology.* 2017;150(2):139-45.
42. Cannon MJ, Hyde TB, and Schmid DS. Review of cytomegalovirus shedding in bodily fluids and relevance to congenital cytomegalovirus infection. *Reviews in medical virology.* 2011;21(4):240-55.
43. Lim EY, Jackson SE, and Wills MR. The CD4+ T Cell Response to Human Cytomegalovirus in Healthy and Immunocompromised People. *Front Cell Infect Microbiol.* 2020;10:202-.
44. Cicin-Sain L, and Arens R. Exhaustion and Inflation at Antipodes of T Cell Responses to Chronic Virus Infection. *Trends in Microbiology.* 2018;26(6):498-509.
45. Collins PL, Cella M, Porter SI, Li S, Gurewitz GL, Hong HS, et al. Gene Regulatory Programs Conferring Phenotypic Identities to Human NK Cells. *Cell.* 2019;176(1):348-60.e12.
46. Fujimoto Y, Tu L, Miller AS, Bock C, Fujimoto M, Doyle C, et al. CD83 Expression Influences CD4+ T Cell Development in the Thymus. *Cell.* 2002;108(6):755-67.
47. García-Martínez LF, Appleby MW, Staehling-Hampton K, Andrews DM, Chen Y, McEuen M, et al. A Novel Mutation in CD83 Results in the Development of a Unique Population of CD4⁺ T Cells. *The Journal of Immunology.* 2004;173(5):2995-3001.
48. Lüthje K, Cramer SO, Ehrlich S, Veit A, Steeg C, Fleischer B, et al. Transgenic expression of a CD83-immunoglobulin fusion protein impairs the development of immune-competent CD4-positive T cells. *European Journal of Immunology.* 2006;36(8):2035-45.
49. Hertoghs KM, Moerland PD, van Stijn A, Remmerswaal EB, Yong SL, van de Berg PJ, et al. Molecular profiling of cytomegalovirus-induced human CD8+ T cell differentiation. *The Journal of clinical investigation.* 2010;120(11):4077-90.

50. Hansen SG, Strelow LI, Franchi DC, Anders DG, and Wong SW. Complete sequence and genomic analysis of rhesus cytomegalovirus. *Journal of virology.* 2003;77(12):6620-36.
51. Reynolds AE, and Enquist LW. Biological interactions between herpesviruses and cyclooxygenase enzymes. *Reviews in Medical Virology.* 2006;16(6):393-403.
52. Zhu H, Cong J-P, Yu D, Bresnahan WA, and Shenk TE. Inhibition of cyclooxygenase 2 blocks human cytomegalovirus replication. *Proceedings of the National Academy of Sciences.* 2002;99(6):3932-7.
53. Slobedman B, Barry PA, Spencer JV, Avdic S, and Abendroth A. Virus-encoded homologs of cellular interleukin-10 and their control of host immune function. *Journal of virology.* 2009;83(19):9618-29.
54. Lockridge KM, Zhou S-S, Kravitz RH, Johnson JL, Sawai ET, Blewett EL, et al. Primate Cytomegaloviruses Encode and Express an IL-10-like Protein. *Virology.* 2000;268(2):272-80.
55. Kotenko SV, Saccani S, Izotova LS, Mirochnitchenko OV, and Pestka S. Human cytomegalovirus harbors its own unique IL-10 homolog (cmvIL-10). *Proceedings of the National Academy of Sciences.* 2000;97(4):1695.
56. Fiorentino DF, Zlotnik A, Mosmann T, Howard M, and O'garra A. IL-10 inhibits cytokine production by activated macrophages. *The Journal of Immunology.* 1991;147(11):3815-22.
57. Hart PH, Vitti GF, Burgess DR, Whitty GA, Piccoli DS, and Hamilton JA. Potential antiinflammatory effects of interleukin 4: suppression of human monocyte tumor necrosis factor alpha, interleukin 1, and prostaglandin E2. *Proceedings of the National Academy of Sciences.* 1989;86(10):3803-7.
58. te Velde A, Huijbens R, Heije K, de Vries J, and Figdor C. Interleukin-4 (IL-4) inhibits secretion of IL-1 beta, tumor necrosis factor alpha, and IL-6 by human monocytes. *Blood.* 1990;76(7):1392-7.
59. Chan A, Baird M, Mercer AA, and Fleming SB. Maturation and function of human dendritic cells are inhibited by orf virus-encoded interleukin-10. *Journal of General Virology.* 2006;87(11):3177-81.
60. Mocellin S, Marincola F, Riccardo Rossi C, Nitti D, and Lise M. The multifaceted relationship between IL-10 and adaptive immunity: putting together the pieces of a puzzle. *Cytokine & Growth Factor Reviews.* 2004;15(1):61-76.
61. Musso T, Calosso L, Zucca M, Millesimo M, Ravarino D, Giovarelli M, et al. Human Monocytes Constitutively Express Membrane-Bound, Biologically Active, and Interferon-γ–Upregulated Interleukin-15. *Blood.* 1999;93(10):3531-9.
62. Zhang X, Sun S, Hwang I, Tough DF, and Sprent J. Potent and Selective Stimulation of Memory-Phenotype CD8+ T Cells In Vivo by IL-15. *Immunity.* 1998;8(5):591-9.
63. Martinet V, Tonon S, Torres D, Azouz A, Nguyen M, Kohler A, et al. Type I interferons regulate eomesodermin expression and the development of unconventional memory CD8(+) T cells. *Nature communications.* 2015;6:7089.
64. Correia MP, Costa AV, Uhrberg M, Cardoso EM, and Arosa FA. IL-15 induces CD8+ T cells to acquire functional NK receptors capable of modulating cytotoxicity and cytokine secretion. *Immunobiology.* 2011;216(5):604-12.
65. Correia MP, Stojanovic A, Bauer K, Juraeva D, Tykocinski LO, Lorenz HM, et al. Distinct human circulating NKp30(+)FcepsilonRIgamma(+)CD8(+) T cell population exhibiting high natural killer-like antitumor potential. *Proc Natl Acad Sci U S A.* 2018;115(26):E5980-e9.
66. Crough T, and Khanna R. Immunobiology of human cytomegalovirus: from bench to bedside. *Clin Microbiol Rev.* 2009;22(1):76-98.
67. Ratzinger G, Baggers J, de Cos MA, Yuan J, Dao T, Reagan JL, et al. Mature human Langerhans cells derived from CD34+ hematopoietic progenitors stimulate greater

cytolytic T lymphocyte activity in the absence of bioactive IL-12p70, by either single peptide presentation or cross-priming, than do dermal-interstitial or monocyte-derived dendritic cells. *J Immunol.* 2004;173(4):2780-91.
68. Busch M, Herzmann C, Kallert S, Zimmermann A, Höfer C, Mayer D, et al. Lipoarabinomannan-Responsive Polycytotoxic T Cells Are Associated with Protection in Human Tuberculosis. *Am J Respir Crit Care Med.* 2016;194(3):345-55.
69. Barrenäs F, Hansen SG, Law L, Driscoll C, Green RR, Smith E, et al. Sustained IL-15 response signature predicts RhCMV/SIV vaccine efficacy. *bioRxiv.* 2021:2021.01.11.426199.
70. Rolot M, Dougall AM, Chetty A, Javaux J, Chen T, Xiao X, et al. Helminth-induced IL-4 expands bystander memory CD8(+) T cells for early control of viral infection. *Nature communications.* 2018;9(1):4516.
71. Barbarin A, Cayssials E, Jacomet F, Nunez NG, Basbous S, Lefevre L, et al. Phenotype of NK-Like CD8(+) T Cells with Innate Features in Humans and Their Relevance in Cancer Diseases. *Frontiers in immunology.* 2017;8:316.
72. Wickham H. ggplot2: Elegant Graphics for Data Analysis. 2016.
73. Bougeard S, and Dray S. Supervised Multiblock Analysis in R with the ade4 Package. *2018.* 2018;86(1):17.
74. Jari Oksanen FGB, Michael Friendly, Roeland Kindt, Pierre Legendre,, Dan McGlinn PRM, R. B. O'Hara, Gavin L. Simpson, Peter Solymos, M. Henry, and H. Stevens ESaHW. vegan: Community Ecology Package. 2019.
75. Kassambara A. fastqcr: Quality Control of Sequencing Data. 2019.
76. Pouzat C. STAR: Spike Train Analysis with R. 2012.
77. Robinson MD, McCarthy DJ, and Smyth GK. edgeR: a Bioconductor package for differential expression analysis of digital gene expression data. *Bioinformatics (Oxford, England).* 2010;26(1):139-40.

FIGURES AND FIGURE LEGENDS

Figure 1

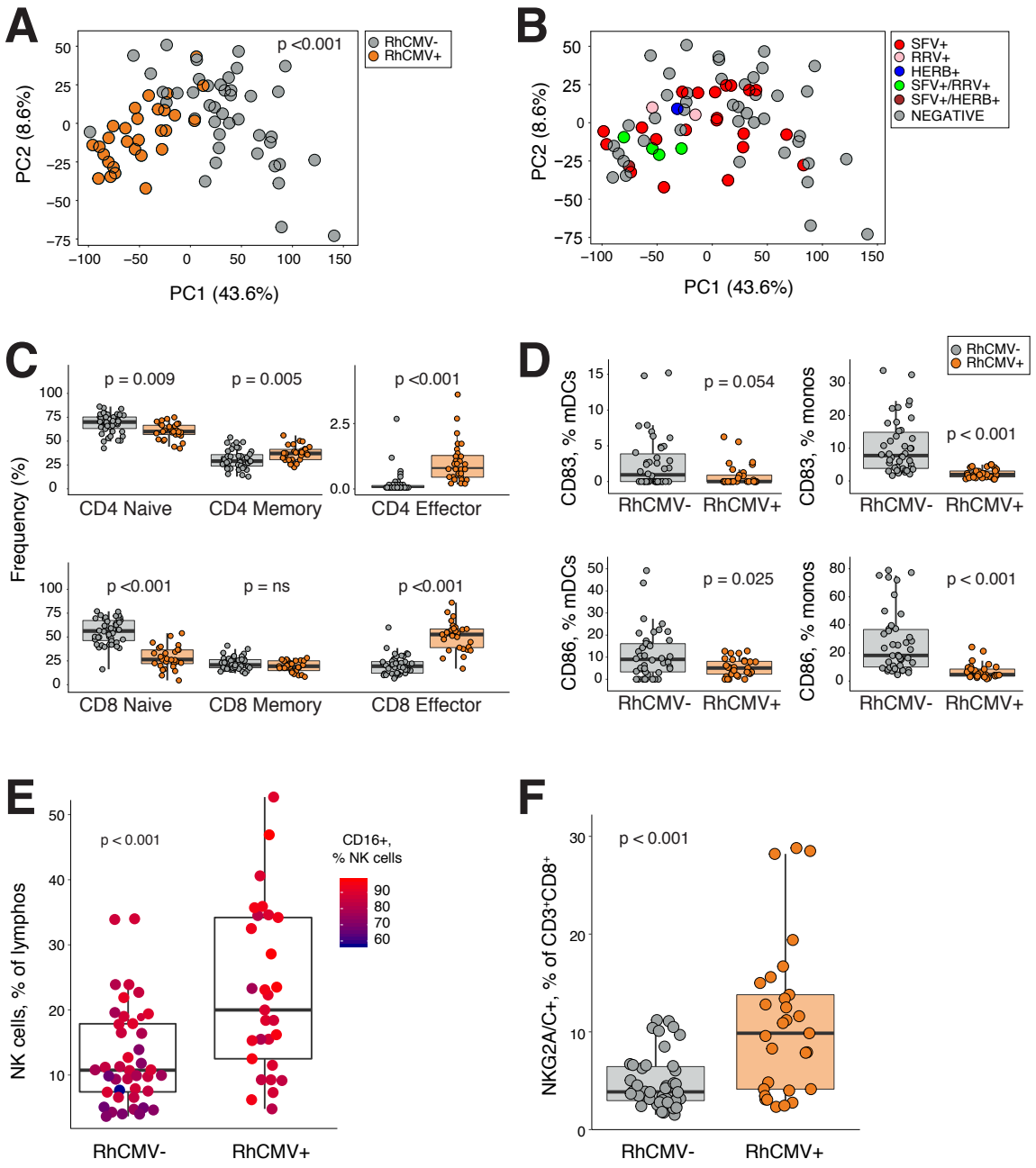

Figure 1. Extensive effects of RhCMV on the macaque immune system. (**A**) Principal component analysis (PCA) summarizing variability in all immune parameters measured by flow cytometry. Dot plots represent values along the first and second principal-

component axes for RhCMV- macaques (grey dots) and RhCMV+ macaques (orange dots). (**B**) PCA plot with dots colored according to presence of other common viral infections: simian foamy virus (SFV; red dots), rhesus rhadinovirus (RRV; pink dots), herpes B virus (HERB; blue dots), SFV^+ and RRV^+ (green dots), SFV^+ and $HERB^+$ (brown dots) and seronegative (gray dots). (**C**) Percentage of naïve ($CD28^+CD95^-$), memory ($CD28^+CD95^+$) and effector ($CD28^-CD95^+$) cells among $CD4^+$ and $CD8^+$ T cells in RhCMV- and RhCMV+ groups. (**D**) Percentage of $CD83^+$ and $CD86^+$ among mDCs ($CD3^-CD20^-CD16^-CD14^-HLADR^+CD11c^+CD123^-$) and monocytes ($CD3^-CD20^-HLADR^+CD14^+$) in RhCMV- and RhCMV+ groups. (**E**) Percentage of NK cells ($CD3^-CD20^-CD8^+NKG2A^+$) in RhCMV- and RhCMV+ groups, colored according to the fraction of NK cells that were $CD16^+$. (**F**) Percentage of NKG2A/C^+CD8^+ CTLs ($CD3^+CD8^+NKG2A^+$) in RhCMV- and RhCMV+ groups. Peripheral blood immunophenotypes were characterized in 42 RhCMV- and 29 RhCMV+ rhesus macaques. Boxplots show the median value, 25^{th} and 75^{th} quartile and the range of values. Permutational MANOVA (function *vegan::adonis*) was used to assess correlations between dissimilarity of samples and RhCMV serostatus in panel A. Wilcoxon rank-sum tests were used to calculate p values in panels C-G.

Figure 2

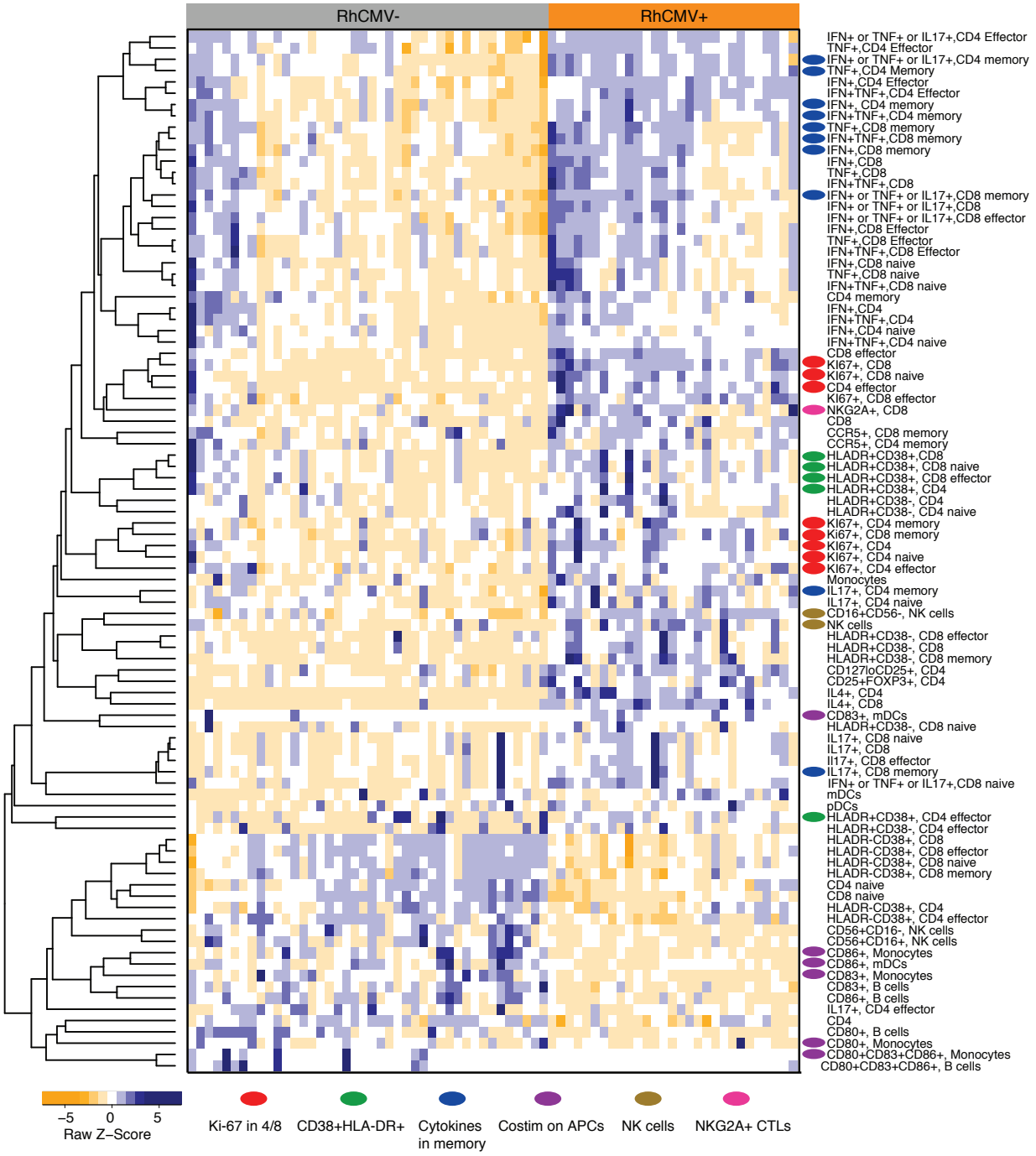

Figure 2. Heatmap of immune phenotypes differently expressed by RhCMV groups.

Wilcoxon rank sum tests were used to identify immune subsets found to be significantly

different between RhCMV+ and RhCMV- groups. Immune cell subsets that were found significantly different between groups ($p<0.05$) were included to generate the heatmap.

Figure 3

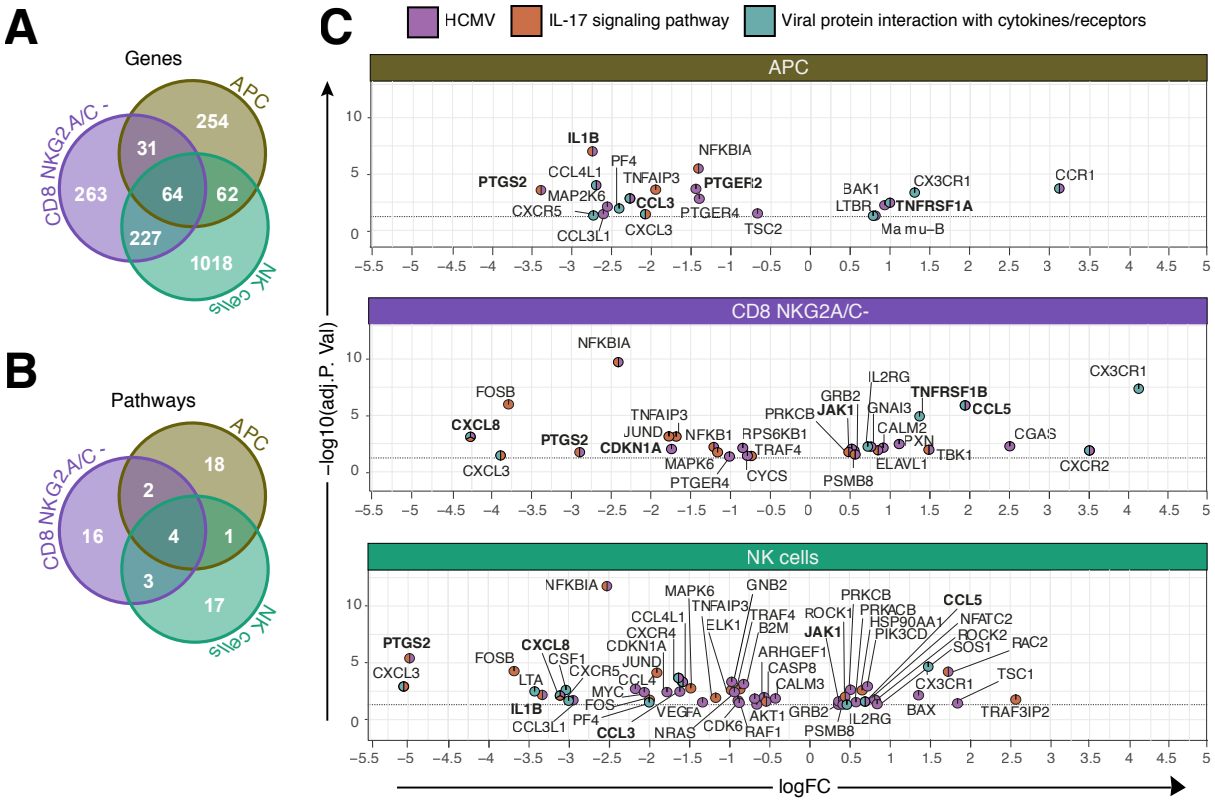

Figure 3. Gene expression profiles of dendritic cells, NK cells, and T cells in RhCMV- and RhCMV+ rhesus macaques. (**A**) Venn diagram showing differently expressed genes ($p_{adj}<0.05$) in three sorted cell types examined for RhCMV- and RhCMV+ macaques. (**B**) Venn diagram showing top-25 significant ($p<0.05$) KEGG pathways. (**C**) Volcano-plot representations of differentially expressed genes in the indicated KEGG pathways among $CD11c^+$ DCs (top), $NKG2A/C^-CD8^+$ T cells (middle), or NK cells (bottom) in RhCMV+ and RhCMV- macaques. Each colored pie slice indicates membership of the corresponding gene in the KEGG pathway corresponding to that color

in the legend. Transcriptomic analysis was performed of flow-sorted cells types from 6 RhCMV+ and 6 RhCMV- rhesus macaques. Differential expression analyses were conducted using the limma-voom Bioconductor pipeline, using a statistical model incorporating the flow-sorted cell population, RhCMV serostatus, and fragmentation time.

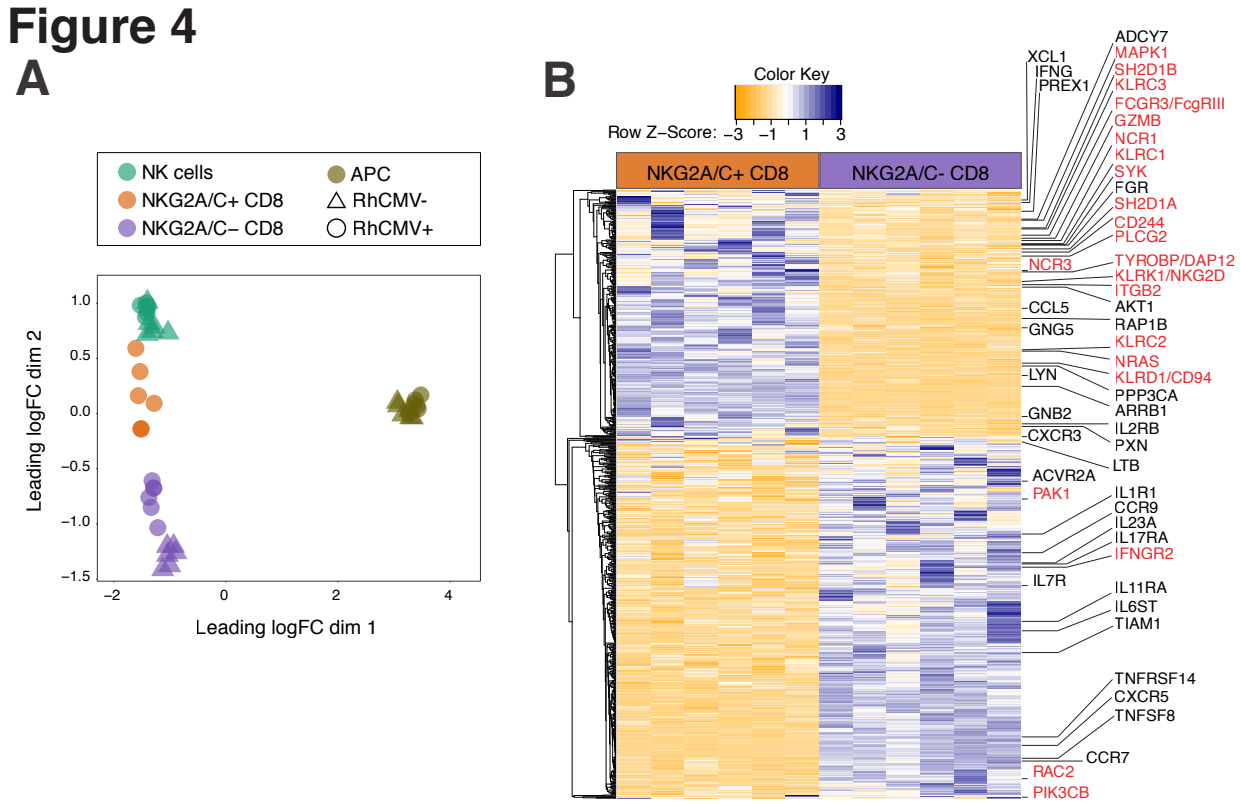

Figure 4. Gene expression of flow-sorted NKG2A/C^{+}CD8^{+} T cells. (A) Multidimensional scaling plot of transcript abundances using distances based on log2-fold differences. (**B**) Heatmap showing scaled values for transcripts that were found to be statistically different (p_{adj}<0.05) between NKG2A/C^{+} and NKG2A/C^{-} CD8^{+} T cells in 6 RhCMV+ macaques.

Figure 5

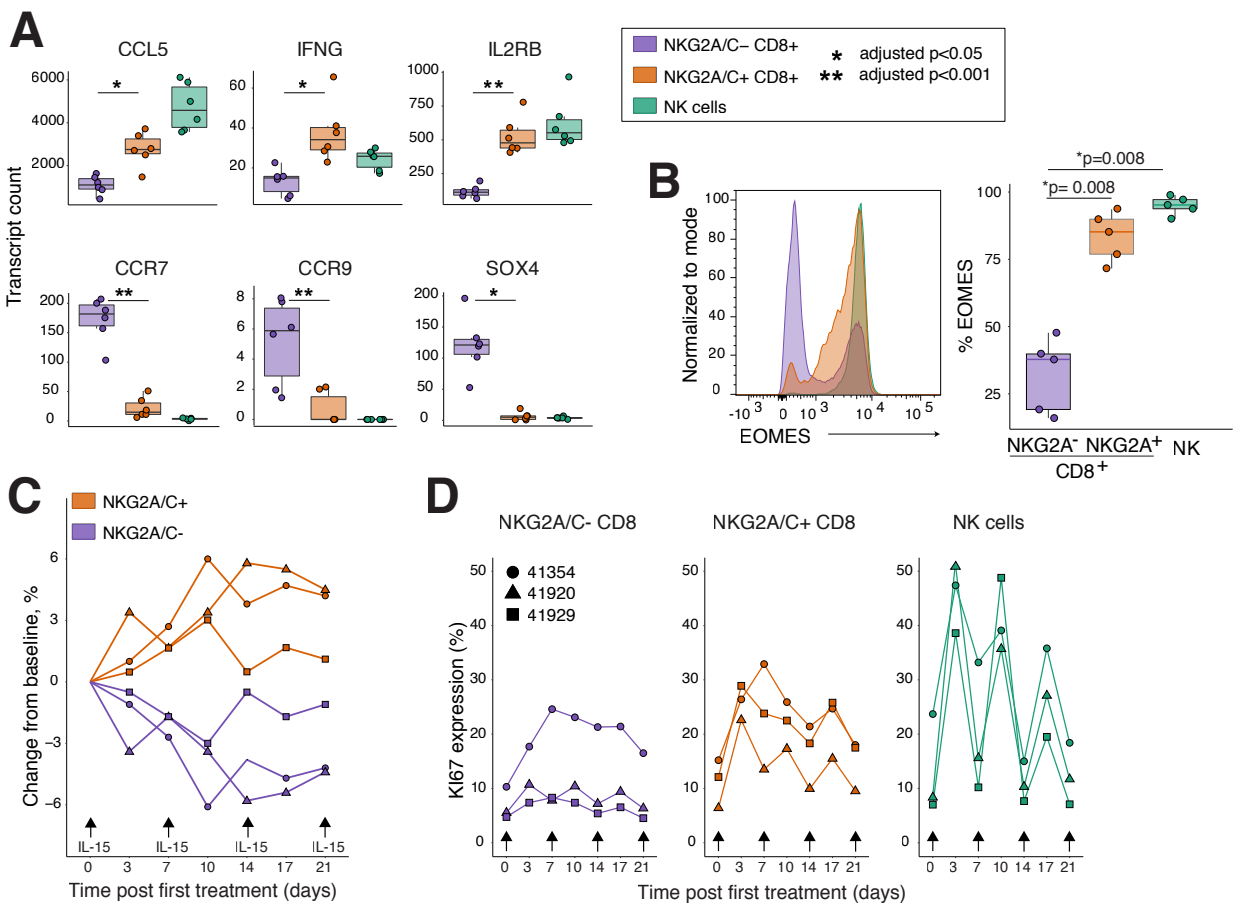

Figure 5. NKG2A/C^{+} CD8^{+} T cells exhibit transcriptional and functional features of T_{VM}'s. (**A**) Abundance of transcripts commonly expressed by T_{VM} cells in sorted cell populations from 6 RhCMV+ and 6 RhCMV- rhesus macaques. (**B, Left**) Representative histogram showing expression of EOMES among gated NKG2A/C^{+}CD8^{+} T cells, NKG2A/C^{-}CD8^{+} T cells or NK cells. (**Right**) Percentage of EOMES^{+} in the three gated populations from 5 different macaques. Dynamics (**C**) and Ki-67 expression **(D)** of NKG2A/C^{+}CD8^{+}, NKG2A/C^{-}CD8^{+} T cells and NK cells following treatment of 3 RhCMV+ rhesus macaques with recombinant IL-15 (10ug/Kg) and IL-15Rα (40ug/Kg). Boxplots show the median value, 25th and 75th quartile and the range of values; Wilcoxon signed-rank tests were used to compare values.

Figure 6

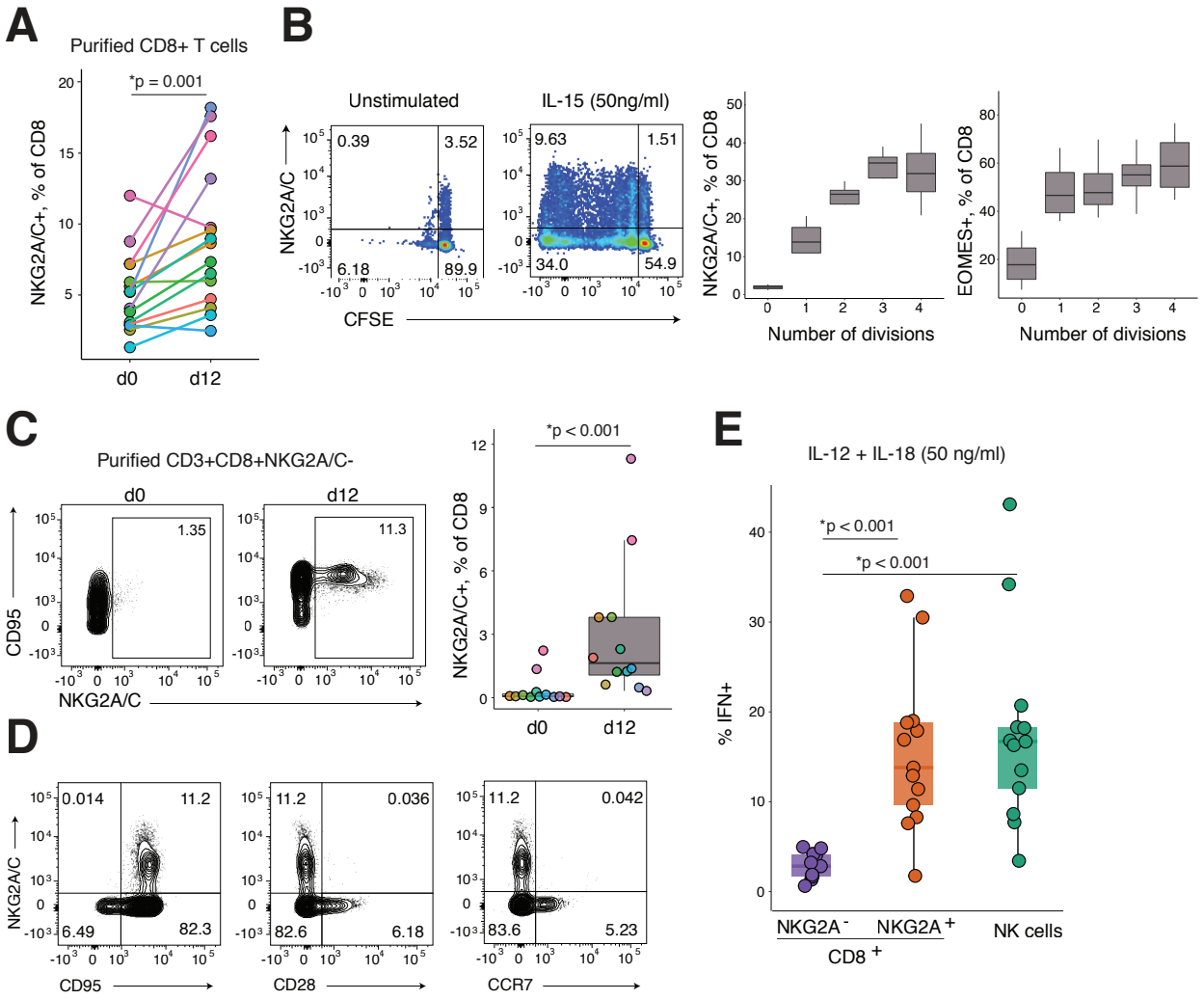

Figure 6. NKG2A/C^{+} CD8^{+} T cells exhibit functional features of T_{VM}'s. (**A-B**) Purified CD8^{+} T cells from 15 RhCMV+ rhesus macaques were cultured for 12 days with IL-15 (50ng/ml). (**A**) Percentage of NKG2A-expressing CD8^{+} T cells on day 0 or 12. (**B, Left**) Representative plots showing NKG2A expression on dividing cells, which are marked by carboxyfluorescein succinimidyl ester (CFSE), on day 12 in unstimulated and IL-15-stimulated cultures. (**Right**) Graph showing the increase in NKG2A and EOMES expression on CD8^{+} T cells gated by division number (according to CFSE dilution), boxplots show the median value, 25th and 75th quartile and the range of values, n=5. (**C-**

D) Purified NKG2A/C$^-$ CD8$^+$ CTLs from 12 RhCMV+ rhesus macaques were cultured for 12 days with IL-15 (50ng/ml). (**C, Left**) Representative plots showing NKG2A expression on day 0 and 12. (**Right**) Percentage of NKG2A-expressing CD8$^+$ T cells on day 0 or 12. (**D**) Flow cytometry plots showing NKG2A/C, CD95, CD28 and CCR7 on day 12. (**E**) PBMCs from 13 RhCMV+ rhesus macaques were cultured for 48h with IL-12 and IL-18**;** IFN-ɣ expression was analyzed after gating on NKG2A/C$^+$CD8$^+$ T cells, NKG2A/C$^-$CD8$^+$ T cells, or NK cells. The frequencies of IFN-ɣ-expressing cells among NKG2A/C$^+$CD8$^+$ T cells when cultured in medium alone was lower than 1.6%. Boxplots show the median value, 25th and 75th quartile and the range of values; Wilcoxon signed-rank tests were used to compare values.

Figure 7

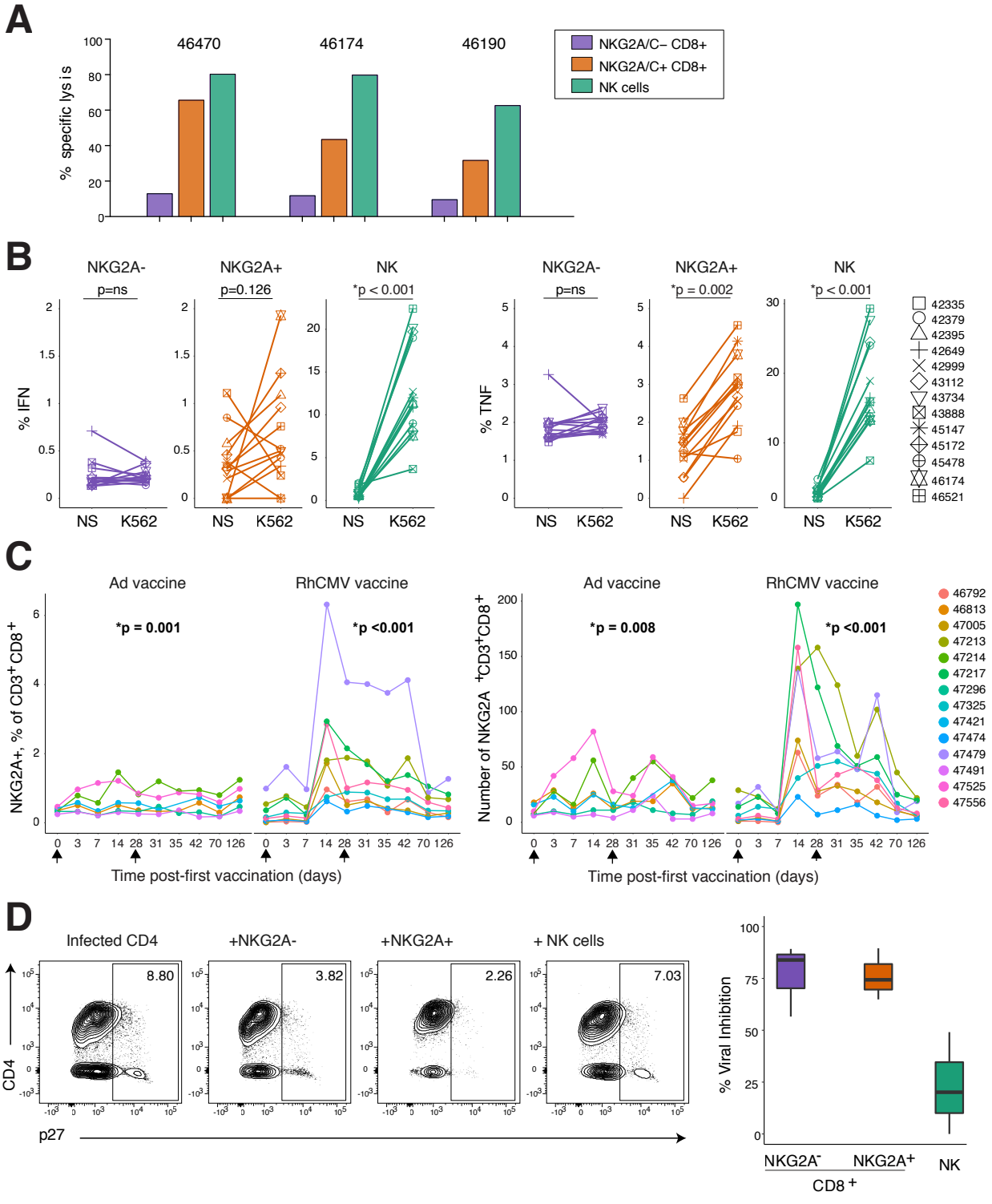

Figure 7. NKG2A/C^{+}CD8^{+} T cells have functional capacities similar to those of NK cells. (**A**) Cytolytic activity of sorted NKG2A/C^{-}CD8^{+} T cells, NKG2A/C^{+}CD8^{+} T cells, or

NK cells from 3 RhCMV+ rhesus macaques against Calcein AM-stained K562 at an E:T ratio of 5:1. (**B**) Resting PBMCs from 13 RhCMV+ rhesus macaques were incubated for 6h alone or with K562. IFN-ɣ and TNF-α expression was analyzed after gating on NKG2A/C$^-$CD8$^+$ T cells, NKG2A/C$^+$CD8$^+$ T cells, or NK cells. Wilcoxon signed-rank tests were used to compare IFN-ɣ and TNF-α values. (**C**) Longitudinal representation of the percentage and absolute numbers of NKG2A/C$^+$CD8$^+$ T cells among lymphocytes before and after vaccination of 14 RhCMV- rhesus macaques. Changes in numbers of NKG2A/C$^+$CD8$^+$ T cells with vaccination time were evaluated with Friedman tests. (**D, left**) Representative FACS plots demonstrating viral outgrowth inhibition (assessed by intracellular Gag p27) observed when autologous, infected CD4$^+$ T cells are cultured alone or in the presence of sorted NKG2A/C$^-$CD8$^+$ T cells, NKG2A/C$^+$CD8$^+$ T cells, or NK cells at an E:T ratio of 1:1. (**Right**) Percentage of viral inhibition. The assay was performed with spleen cells and PBMCs from necropsies, boxplots show the median value, 25th and 75th quartile and the range of values, n=3.

Table 1: Study groups

Assay	Group	Number	Age (Years)	Sex (Males:Females)
Transcriptomic analysis	RhCMV -	6	0.89 ± 0.1 (0.79 – 1.05)	2:4
	RhCMV +	6	2.11 ± 0.06 (2.04 – 2.18)	3:3
***In-vivo* IL-15 responsiveness**	RhCMV +	3	4.61 ± 0.46 (4.36 – 5.16)	3:0
***In-vitro* functional responsiveness**	RhCMV +	25	4.79 ± 2.06 (2.4 – 9.78)	12:13
Vaccination study	RhCMV - (SPF level 2)	14	1.04 ± 0.11 (0.85 – 1.24)	4:10

Data shown as mean ± SD (Range)